Calcineurin regulates the yeast synaptojanin Inp53/Sjl3 during membrane stress

Evan L. Guiney[a], Aaron R. Goldman[a], Joshua E. Elias[b], and Martha S. Cyert[a]
[a]Department of Biology and [b]Department of Chemical and Systems Biology, Stanford University, Stanford, CA 94305

ABSTRACT During hyperosmotic shock, *Saccharomyces cerevisiae* adjusts to physiological challenges, including large plasma membrane invaginations generated by rapid cell shrinkage. Calcineurin, the Ca^{2+}/calmodulin–dependent phosphatase, is normally cytosolic but concentrates in puncta and at sites of polarized growth during intense osmotic stress; inhibition of calcineurin-activated gene expression suggests that restricting its access to substrates tunes calcineurin signaling specificity. Hyperosmotic shock promotes calcineurin binding to and dephosphorylation of the PI(4,5)P_2 phosphatase synaptojanin/Inp53/Sjl3 and causes dramatic calcineurin-dependent reorganization of PI(4,5)P_2-enriched membrane domains. Inp53 normally promotes sorting at the *trans*-Golgi network but localizes to cortical actin patches in osmotically stressed cells. By activating Inp53, calcineurin repolarizes the actin cytoskeleton and maintains normal plasma membrane morphology in synaptojanin-limited cells. In response to hyperosmotic shock and calcineurin-dependent regulation, Inp53 shifts from associating predominantly with clathrin to interacting with endocytic proteins Sla1, Bzz1, and Bsp1, suggesting that Inp53 mediates stress-specific endocytic events. This response has physiological and molecular similarities to calcineurin-regulated activity-dependent bulk endocytosis in neurons, which retrieves a bolus of plasma membrane deposited by synaptic vesicle fusion. We propose that activation of Ca^{2+}/calcineurin and PI(4,5)P_2 signaling to regulate endocytosis is a fundamental and conserved response to excess membrane in eukaryotic cells.

Monitoring Editor
John York
Vanderbilt University

Received: May 29, 2014
Revised: Dec 4, 2014
Accepted: Dec 11, 2014

INTRODUCTION

Cells dynamically maintain their surface by adding membrane through exocytosis and retrieving it through endocytosis. In growing cells, coordination of these processes ensures that surface area increases to keep pace with cellular volume. In contrast, a rapid decrease in cell size generates excess plasma membrane. During hypertonic shock, for example, cells of the budding yeast *Saccharomyces cerevisiae* lose up to 50% their volume, which causes the plasma membrane to buckle and form large, sheet-like invaginations (Kopecka *et al.*, 1973; Morris *et al.*, 1986; Slaninova *et al.*, 2000; Dupont *et al.*, 2010). In response to these extreme conditions, the cell surface is rapidly remodeled, normal morphology is restored, and growth resumes. Much of this regulation must target the actin cytoskeleton, which is essential for both exocytosis and endocytosis in *S. cerevisiae*. However, how these processes are regulated in response to stress is not well understood.

During normal growth, the yeast actin cytoskeleton is polarized; actin cables, which deliver secretory vesicles, and mobile cortical actin patches, which are sites of clathrin-mediated endocytosis (CME) and cell wall synthesis, both concentrate in the growing bud (Mulholland *et al.*, 1994; Utsugi *et al.*, 2002; Pruyne *et al.*, 2004; Kaksonen *et al.*, 2005). Polarized growth is established and maintained through the activity of small G proteins, Cdc42 and Rho1, which are activated by TOR/target of rapamycin and directly regulate exocytosis, cell wall synthesis, and actin polymerization through their targets Sec3, Fks1, protein kinase C, and the formins Bni1 and Bnr1 (Levin, 2011; Loewith and Hall, 2011; Bi and Park, 2012). In response to many types of environmental stress, including heat stress and hypertonic shock, the actin cytoskeleton rapidly reorganizes: within 30 min, actin cables disassemble, halting the delivery of

This article was published online ahead of print in MBoC in Press (http://www.molbiolcell.org/cgi/doi/10.1091/mbc.E14-05-1019) on December 17, 2014.

Address correspondence to: Martha S. Cyert (mcyert@stanford.edu).

Abbreviations used: ADBE, activity-dependent bulk endocytosis; CME, clathrin-mediated endocytosis; CN, calcineurin; PI(4,5)P_2, phosphatidylinositol-4,5-bisphosphate; TGN, *trans*-Golgi network.

secretory vesicles, and actin patches spread throughout the surface of both mother and daughter cells (Chowdhury *et al.*, 1992; Palmer *et al.*, 1992). These depolarized actin patches are presumed to function as sites of cell wall synthesis and endocytosis that repair and restore the cell surface. Indeed, after several hours, the cytoskeleton repolarizes, indicating that the cell has adapted to its new environment and is ready to resume growth (Chowdhury *et al.*, 1992). The composition and function of actin patches in stressed cells are incompletely understood; however, in growing cells, the mechanisms that underlie CME have been well elucidated.

CME occurs through a coordinated series of protein–protein and protein–lipid interactions, which allows incorporation of cargo into a membrane deformation that matures into an endocytic invagination, using force provided by actin polymerization, and is released into the cytoplasm as an endocytic vesicle after membrane scission. A well-defined set of proteins act in temporally discrete modules to carry out these events (Weinberg and Drubin, 2012). Coat proteins, including clathrin, are among the earliest to arrive at endocytic sites (Kaksonen *et al.*, 2005). The coat matures with the arrival of cargo and adaptor proteins such as Sla1 (Mahadev *et al.*, 2007; Di Pietro *et al.*, 2010; Feliciano and Di Pietro, 2012). As the endocytic site matures, actin polymerization begins with recruitment of proteins in the WASP/MYO module (Sun *et al.*, 2006). Actin polymerization drives the actin network and associated actin module proteins (such as Bsp1) into the cytoplasm (Tonikian *et al.*, 2009); the force supplied by actin polymerization promotes formation of a membrane invagination. Scission module proteins are the last to arrive at the mature endocytic site. Actin polymerization, phosphatidylinositol-4,5-bisphosphate ($PI(4,5)P_2$) hydrolysis (carried out by the yeast synaptojanin Inp52/Sjl2), and curvature induced by BAR-domain proteins (Bzz1 and Rvs161/Rvs167) together promote membrane scission and release of an endocytic vesicle (Kishimoto *et al.*, 2011). Regulation of $PI(4,5)P_2$ plays an important role throughout endocytosis, as $PI(4,5)P_2$ recruits proteins to the membrane, increases membrane fluidity, and facilitates curvature (Sun *et al.*, 2007; Liu *et al.*, 2009). In a growing cell, these events occur constitutively and lead to continual formation of endocytic vesicles.

Mammalian cells use many of these same principles to carry out endocytosis. The reliance on a network of SH3-dependent protein–protein interactions is highly conserved, as is the role of $PI(4,5)P_2$ and BAR-domain proteins in membrane invagination (Taylor *et al.*, 2011). However, whereas some core endocytic proteins and regulators are conserved, others are organism specific, and the SH3 network in particular evolved rapidly to conserve overall function rather than preserve the identity of participating proteins (Xin *et al.*, 2013). Other differences between endocytosis in mammalian and yeast cells include the role of actin polymerization, which is apparently not essential for all endocytic pathways in animal cells but is universally required in yeast cells which are under turgor pressure (Aghamohammadzadeh and Ayscough, 2009; Weinberg and Drubin, 2012). In addition, membrane scission depends on the dynamin GTPase in mammals, whereas the role of Vps1, the yeast dynamin relative, in endocytosis is unclear (Shupliakov *et al.*, 1997; Smaczynska-de *et al.*, 2010, 2012; Weinberg and Drubin, 2012).

How does this complex network of endocytic events respond to the challenges presented by hypertonic shock? When exposed to even mild hypertonic conditions, yeast cells immediately lose water, causing a decrease in turgor pressure, which activates the high-osmolarity glycerol (HOG) mitogen-activated protein kinase signaling pathway. HOG signaling increases intracellular glycerol and promotes long-term osmoadaptation (Schaber *et al.*, 2010; Saito and Posas, 2012), but during extreme hypertonic shock, cells lose volume and decrease in size despite maximal activation of the HOG pathway. Although it is not yet clear how the massive plasma membrane invaginations that result from this cell shrinkage are resolved (Kopecka *et al.*, 1973; Morris *et al.*, 1986; Slaninova *et al.*, 2000; Dupont *et al.*, 2010), the endocytic machinery is likely involved. Many endocytic proteins promote the recovery of actin polarization after hyperosmotic shock, and depolarized actin patches may carry out endocytic events that restore the cell surface.

Several observations indicate that the composition of actin patches changes during osmotic stress. Yeast encodes three synaptojanin homologues—Inp51/Sjl1, Inp52/Sjl2, and Inp53/Sjl3 (Singer-Kruger *et al.*, 1998; Stolz *et al.*, 1998). As noted, Inp52 plays a vital role in CME that occurs in the bud during polarized growth (Stefan *et al.*, 2005). In contrast, Inp53, which is closely related to Inp52, localizes to the *trans*-Golgi network (TGN), where it binds to clathrin and mediates endosomal protein sorting, a process that is phosphoinositide dependent (Ha *et al.*, 2001, 2003; Daboussi *et al.*, 2012). However, in response to osmotic stress, Inp53 localizes to actin patches, and overexpression of either Inp53 or its homologue Inp52 hastens repolarization of the actin cytoskeleton under these conditions (Ooms *et al.*, 2000). Rvs167/amphiphysin and Bzz1/syndapin are also required to restore the polarized actin cytoskeleton after hyperosmotic shock (Bauer *et al.*, 1993; Soulard *et al.*, 2002), and several mutants lacking endocytic proteins are defective for growth in hypertonic conditions (including *inp52*Δ, *inp53*Δ, *rvs167*Δ, *sla1*Δ, and *act1-1*; Chowdhury *et al.*, 1992; Srinivasan *et al.*, 1997; Dudley *et al.*, 2005; Yoshikawa *et al.*, 2009). Thus hyperosmotic stress modulates actin patches, and these structures may resolve the membrane invaginations caused by volume loss through stress-specific endocytic events.

Examining the response to hyperosmotic stress may therefore reveal signaling mechanisms that regulate endocytosis. We noted that high osmolarity triggers a rise in cytosolic Ca^{2+} in yeast, mediated in part by release of vacuolar Ca^{2+} through the Yvc1 channel (Denis and Cyert, 2002). To investigate possible targets of this Ca^{2+} signal, we examined whether calcineurin (CN), the conserved Ca^{2+}/calmodulin–activated protein phosphatase and target of the immunosuppressant drugs FK506 and cyclosporine A (Roy and Cyert, 2013), was active during hyperosmotic shock. The CN heterodimer is made up of a catalytic subunit (Cna1 or Cna2) and a required Ca^{2+}-binding regulatory subunit (Cnb1). CN is not active under standard growth conditions but promotes survival during environmental stress conditions, such as high concentrations of Na^+ and Li^+ and high pH (Cyert and Philpott, 2013). In response to a Ca^{2+} signal, Ca^{2+}-bound calmodulin interacts with and activates CN, which must physically associate with its substrates via conserved docking motifs during dephosphorylation (Roy and Cyert, 2009; Grigoriu *et al.*, 2013). CN regulates gene expression by promoting accumulation of the Crz1 transcription factor in the nucleus (Stathopoulos and Cyert, 1997; Stathopoulos-Gerontides *et al.*, 1999) and stimulates specific endocytic events mediated by the α-arrestins Aly1 and Rod1 (O'Donnell *et al.*, 2013; Alvaro *et al.*, 2014). Furthermore, recent systematic identification of CN substrates in yeast revealed several proteins involved in polarized growth and actin regulation, including the CN-interacting protein synaptojanin Inp52 (Goldman *et al.*, 2014).

In this work, we demonstrate that CN accumulates at sites of polarized growth during hyperosmotic shock and dephosphorylates synaptojanin/Inp53 to promote actin polarization and maintain membrane morphology. Localized activation of synaptojanin is also suggested by a dramatic redistribution of $PI(4,5)P_2$ in the membrane observed during osmotic shock that is calcineurin regulated.

Osmotic stress induces Inp53 to associate with multiple endocytic proteins, and some of these interactions are promoted by CN. Synaptojanin is one of only two proteins identified as CN substrates in both yeast and mammals. In neurons, CN dephosphorylates synaptojanin and other proteins, termed dephosphins, to stimulate the activity-dependent bulk endocytosis (ADBE) that follows multiple rounds of synaptic vesicle fusion events (Clayton and Cousin, 2009). We suggest that in both neurons and osmotically stressed yeast cells, a sudden excess of plasma membrane triggers a conserved, CN-regulated response that restores the cell surface.

RESULTS

Calcineurin localizes to sites of polarized growth during hyperosmotic stress

Mammalian cells encode scaffold proteins that interact with CN and substrates to target the phosphatase to specific subcellular compartments. For example, in neurons, AKAP79 localizes CN to L-type Ca^{2+} channels at the plasma membrane (Oliveria *et al*., 2007). In contrast, under standard growth conditions, yeast CN localized diffusely throughout the cell, as visualized in cells expressing the functional Cna1-3x green fluorescent protein (Cna1-3GFP) fusion protein from its endogenous locus (Figure 1A). Because CN is active during environmental stress, we also examined its distribution under a range of stress conditions. These analyses revealed that Cna1-3GFP distribution changed dramatically 10 min after addition of 1.25 M KCl to the growth medium, accumulating at foci throughout the cell body, the bud tip, and the bud neck. Cna2-3GFP, a functionally redundant catalytic subunit isoform, displayed similar localization changes under these conditions (Supplemental Figure S1A). This redistribution of CN was triggered by hypertonic shock, as NaCl (1.25 M), sorbitol (2 M), and KCl (1.25 M) all provoked the same response (Figure 1A), which occurred only during intense hyperosmotic stress (KCl > 0.75 M) and became more pervasive as osmotic strength increased (Supplemental Figure S1B). However, CN remained cytosolic in cells exposed either to 200 mM LiCl, a condition under which CN is required for survival that does not induce hyperosmotic shock (Figure 1A and Supplemental Figure S1C), or 50 mM $CaCl_2$, which activates CN-dependent transcription without inducing osmotic stress (Figure 1A). Furthermore, hypertonic shock caused redistribution of Cna1-3GFP in cells treated with the CN inhibitor FK506 (Figure 1A) and in a CN-deficient mutant that lacks the regulatory subunit (*cnb1*; Supplemental Figure S1D). Therefore the cellular localization of CN changes specifically in response to intense hyperosmotic shock, and this redistribution in independent of CN activity. Surprisingly, the observed changes in CN localization did not depend on the HOG pathway and occurred robustly in *hog1*, *pbs2*, and *ssk2* mutants exposed to hyperosmotic challenge (Supplemental Figure S1E). The requirement for intense osmotic shock to redistribute CN also distinguishes this response from HOG pathway activation, which occurs at much lower osmolarities (Schaber *et al*., 2010).

After hyperosmotic shock, CN localization to cytoplasmic foci, the bud neck, and the bud tip followed different kinetics ($p < 0.0001$; Figure 1C). Ten minutes after hyperosmotic shock, CN localized to foci in 100% of cells, but this pattern was transient and disappeared completely by 4 h. Some foci showed colocalization with clathrin (Chc1–red fluorescent protein [RFP]; Supplemental Figure S1G). CN-containing foci also showed partial colocalization with the actin-binding protein Abp1-RFP, which serves as a marker for endocytic patches (Supplemental Figure S2A). In contrast, CN localization to the bud tip and bud neck peaked later (60% of budded cells at 30 min) and was more prolonged than the observed foci; a significant fraction of cells retained Cna1-3GFP at the bud neck after 4 h of hyperosmotic stress (Figure 1, B and C). Thus cellular CN foci may reflect a response to hyperosmotic stress that is functionally distinct from its localization to the bud neck and bud tip. Overall, changes in CN distribution suggest that its interactions substantially change during hyperosmotic shock and in particular include colocalization with the actin cytoskeleton.

In *S. cerevisiae*, the bud tip and bud neck are sites of polarized growth, which stimulate polymerization and organization of the polarized actin cables that deliver the bulk of cellular secretory vesicles to the bud (Pruyne *et al*., 2004). To determine whether the actin cytoskeleton is required for polarized localization of CN, we exposed a uniform population of large-budded cells, obtained after release from mating pheromone arrest, to osmotic stress. Under these conditions, CN localization to the bud neck was extremely consistent (Figure 1D). Fluorescence intensity of Cna1-3GFP in a line along the mother/bud axis was averaged, and after a 10-min hyperosmotic shock, two clear Cna1-3GFP peaks on either side of the bud neck were visible (Figure 1E; $N = 104$ cells). However, depolymerization of the actin cytoskeleton with latrunculin A abolished localization of Cna1-3GFP to the bud neck (Figure 1E and Supplemental Figure S1F). Thus localization of CN to sites of polarized growth requires an intact actin cytoskeleton.

Hypertonic shock induces distinct calcineurin signaling events

A role for CN in the response to hyperosmotic stress had not been previously appreciated. Although CN is required for survival during both NaCl and LiCl stress, in part due to CN-dependent expression of the *ENA1*-encoded plasma membrane Na^+/Li^+-ATPase (Mendoza *et al*., 1994), loss of CN has no effect on long-term growth under nontoxic hyperosmotic stresses such as KCl (Supplemental Figure S1C). Despite this, the cytoplasmic Ca^{2+} signal (Denis and Cyert, 2002) and dramatic localization changes induced by hyperosmotic stress suggested that CN might function during the early response to these conditions.

Under many environmental conditions, CN ensures cell survival by activating the Crz1 transcription factor, promoting its translocation from the cytosol to the nucleus (Stathopoulos and Cyert, 1997; Stathopoulos-Gerontides *et al*., 1999). Therefore we measured CN-Crz1–dependent expression of *4x-CDRE-LacZ*, a reporter gene controlled by the Crz1- binding site, during hyperosmotic stress. As expected, addition of $CaCl_2$ caused a 40-fold induction of *CDRE-LacZ* expression (Figure 2). In contrast, no activation of CN-Crz1 signaling was observed in response to hyperosmotic stress despite the increase in intracellular Ca^{2+} that occurs under these conditions (Denis and Cyert, 2002). Instead, hyperosmotic stress blocked Ca^{2+}-dependent activation of Crz1 (Figure 2). This surprising effect suggested that hypertonic conditions inhibit CN/Crz1 signaling, perhaps in part by relocalizing CN and preventing its access to Crz1.

Thus several unique features of CN signaling, including its localization to sites of polarized growth and failure to activate Crz1-dependent gene expression, suggest that hypertonic shock activates distinct calcineurin-regulated events. We next sought to identify these CN-regulated processes and substrates.

Calcineurin regulates actin rearrangements during hyperosmotic shock

The depolarization and subsequent repolarization of the actin cytoskeleton is a prominent and acute cellular response to hyperosmotic shock (Chowdhury *et al*., 1992). CN localization to sites of polarized growth and partial colocalization with Abp1 suggested that the phosphatase might regulate the actin cytoskeleton during hyperosmotic shock. To test this idea, cells were exposed to

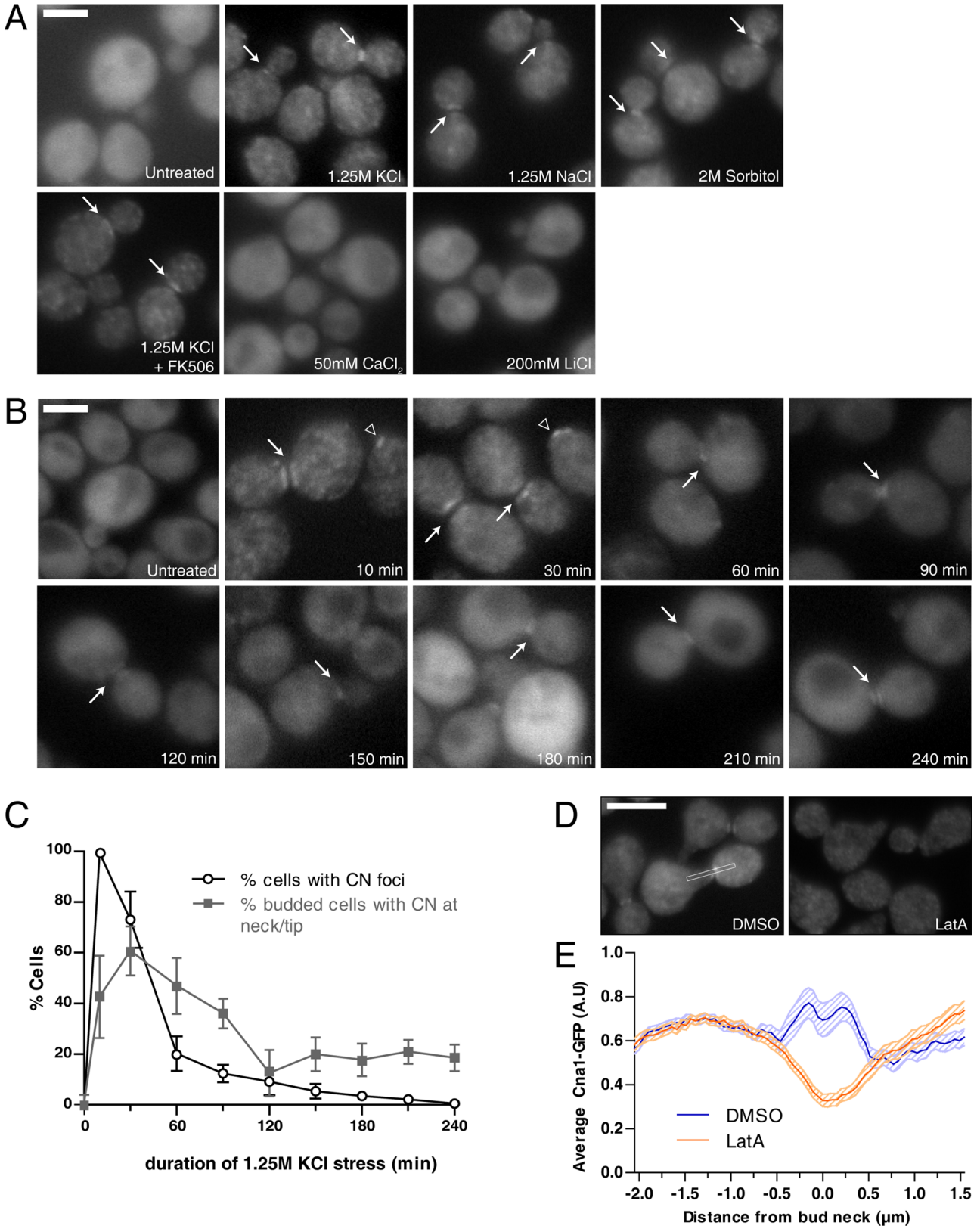

FIGURE 1: Calcineurin localizes to sites of polarized growth during hyperosmotic stress. (A) Micrographs of wild-type (BY4741) cells with integrated Cna1-3GFP. Cells were treated as indicated for 10 min before visualization; where indicated, cells were pretreated with 1 μg/ml FK506 for 30 min; scale bars, 5 μm. (B) Localization of Cna1-3GFP during prolonged 1.25 M KCl stress; arrows: bud neck, arrowheads: bud tip, scale bars, 5 μm. (C) Quantification of percentage of cells with foci or bud neck/bud tip CN during 1.25 M KCl stress; $N > 100$ at each time point. Loss of foci and neck/tip localization was evaluated by fitting one-phase exponential decay, yielding $t_{1/2}$ foci = 26.8 ± 0.6 min, $t_{1/2}$ neck/tip = 36 ± 3.4 min;

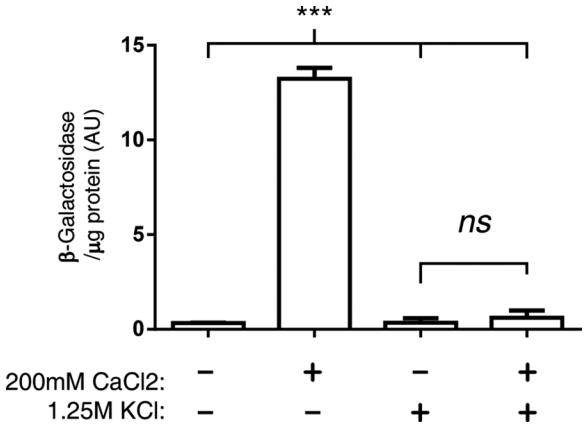

FIGURE 2: Calcineurin-activated gene expression is inhibited during hyperosmotic shock. Ca^{2+}/CN–dependent Crz1 transcription was measured with a *CDRE-LacZ* reporter. β-Galactosidase activity normalized to protein concentration is reported. Cells were treated for 90 min with 200 mM $CaCl_2$ and/or 1.25 M KCl as indicated. Error bars are SD; ***$p < 0.001$.

1.25 M KCl, fixed at 30-min intervals, stained for actin with rhodamine–phalloidin, and polarization quantified using image-analysis software (see *Materials and Methods*). Control cells were maximally depolarized (50%) 2 h after exposure to 1.25 M KCl, and polarity was largely restored by 4 h (Figure 3, A and B). Inactivation of CN with FK506 exacerbated depolarization at 120 and 150 min; however, as in control cells, polarity was reestablished by 4 h (Figure 3, A and B). Analyzing the distributions of cellular fluorescence ratios at 120 and 150 min after hyperosmotic shock showed that FK506 significantly decreased polarization compared with the control (Figure 3C; $p < 10^{-9}$). Thus CN promotes repolarization of the actin cytoskeleton after hyperosmotic challenge.

Inp53 is a calcineurin substrate

Because the altered subcellular distribution of CN likely reflected a change in protein–protein interactions, we sought to identify proteins whose association with CN increased during hyperosmotic stress. Mass spectrometry was used to identify proteins that copurified with endogenously expressed, epitope-tagged CN (Cna2-TEV-ZZ) isolated from either unstressed cells or cells exposed to 1.25 M KCl, as compared with purifications from untagged cells, which controlled for nonspecific background. These analyses suggested a possible interaction between CN and Inp53/Sjl3, one of three yeast synaptojanins (Figure 4A; Srinivasan *et al.*, 1997; Stolz *et al.*, 1998), which was enhanced during hyperosmotic stress. In unstressed cells, Inp53 contributes to protein sorting at the TGN but localizes to actin patches and stimulates repolarization of the actin cytoskeleton during osmotic stress (Ooms *et al.*, 2000). Thus we hypothesized that CN might promote actin polarization during hyperosmotic stress by regulating Inp53.

To examine CN-Inp53 interaction, we isolated glutathione *S*-transferase (GST)–Inp53 from yeast extracts and confirmed that it copurified with Cna2 and that more Cna2 associated with GST-Inp53 purified from cells exposed to hyperosmotic stress (Figure 4B). Inp53 contains two distinct phosphoinositide phosphatase domains (SAC and IP5Pase; Guo *et al.*, 1999; Figure 4A), as well as a C-terminal proline-rich tail domain (PRD) that mediates protein–protein interactions (Ha *et al.*, 2003). Expressing each domain of Inp53 separately and assessing its copurification with CN established that the CN-Inp53 interaction was mediated by the SAC domain (unpublished data). CN interacts with many of its substrates and regulators via a conserved PxIxIT docking motif (Roy and Cyert, 2009). A match to the PxIxIT consensus (Goldman *et al.*, 2014), $PRVQIT_{300\text{-}305}$, occurs in a surface-exposed loop of the Inp53 SAC domain (Manford *et al.*, 2010), as well as in this region of Inp52 and synaptojanin homologues from a broad range of fungal species (Figure 4A and Supplemental Figure S3C; Wapinski *et al.*, 2007). Mutation of this sequence to ARAQAA substantially reduced, but did not completely eliminate, copurification of CN with Inp53 (Figure 4B). This mutated allele is hereafter referred to as $Inp53^{ARAQAA}$. Despite the physical interaction between Inp53 and CN, substantial colocalization between Cna1-3GFP and Inp53-3RFP was not observed during osmotic shock (Supplemental Figure S2, B and D), nor did disruption of CN binding with $Inp53^{ARAQAA}$ block Cna1-3GFP localization to sites of polarized growth (Supplemental Figure S2, C and D).

Purification of GST-Inp53 from cell extracts revealed that its phosphorylation increased in cells exposed to hyperosmotic stress (Figure 4C). Examination of each Inp53 domain showed that only phosphorylation of the PRD increased under these conditions (Supplemental Figure S3A). Furthermore, enhanced PRD phosphorylation was observed in extracts of FK506-treated cells, demonstrating that CN regulates PRD phosphorylation both in the presence and absence of hyperosmotic stress. Surprisingly, this phosphorylation was not due to Hog1, as osmotic stress induced–phosphorylation of PRD appeared to be equivalent in wild-type (WT) and *hog1* yeast (Supplemental Figure S3B). No effect of FK506 on the phosphorylation of full-length GST-Inp53 was detected, possibly due to its large size and high level of overall phosphorylation. Thus, during hyperosmotic stress, the Inp53 PRD becomes heavily phosphorylated, and CN, also active under these conditions, promotes its dephosphorylation.

Taken together, the phosphorylation and interaction data strongly suggest that CN directly regulates Inp53 in vivo and that their association is specifically enhanced during hyperosmotic stress. Furthermore, because the CN-Inp53 interaction is disrupted in $Inp53^{ARAQAA}$, this allele should display impaired regulation by CN when expressed in vivo.

Calcineurin promotes actin polarization via regulation of Inp53

To examine regulation of Inp53 by CN in the absence of partially redundant Inp51 and Inp52, we used an *inp51 inp52 inp53* triple mutant; the viability of this strain (hereafter *inp*ΔΔΔ) was maintained by a galactose-regulated copy of *INP53* that was stably integrated into the genome. As expected, *inp*ΔΔΔ cells expressing a control vector were inviable when grown in dextrose-containing medium (Figure 5A). *INP53* or $INP53^{ARAQAA}$ was introduced into *inp*ΔΔΔ on either a low- or high-copy plasmid and provided the sole source of synaptojanin during growth on dextrose. In the

$plateau_{(foci)} = 1.2 \pm 0.4\%$, $plateau_{(neck/tip)}$ $15.5 \pm 0.9\%$; $p < 0.0001$, extra sum-of-squares *F* test. Error bars are SD. (D) Representative micrographs; scale bar, 5 µm. (E) Average Cna1-3GFP intensity at bud neck along the mother–bud axis (example: D, open bar), centered at the bud neck; cells were synchronized and treated with latrunculin A (LatA) or vehicle as described in *Materials and Methods*, then stressed for 10 min with 1.25 M KCl. Error, SEM; $N = 104$ (LatA), 114 (DMSO).

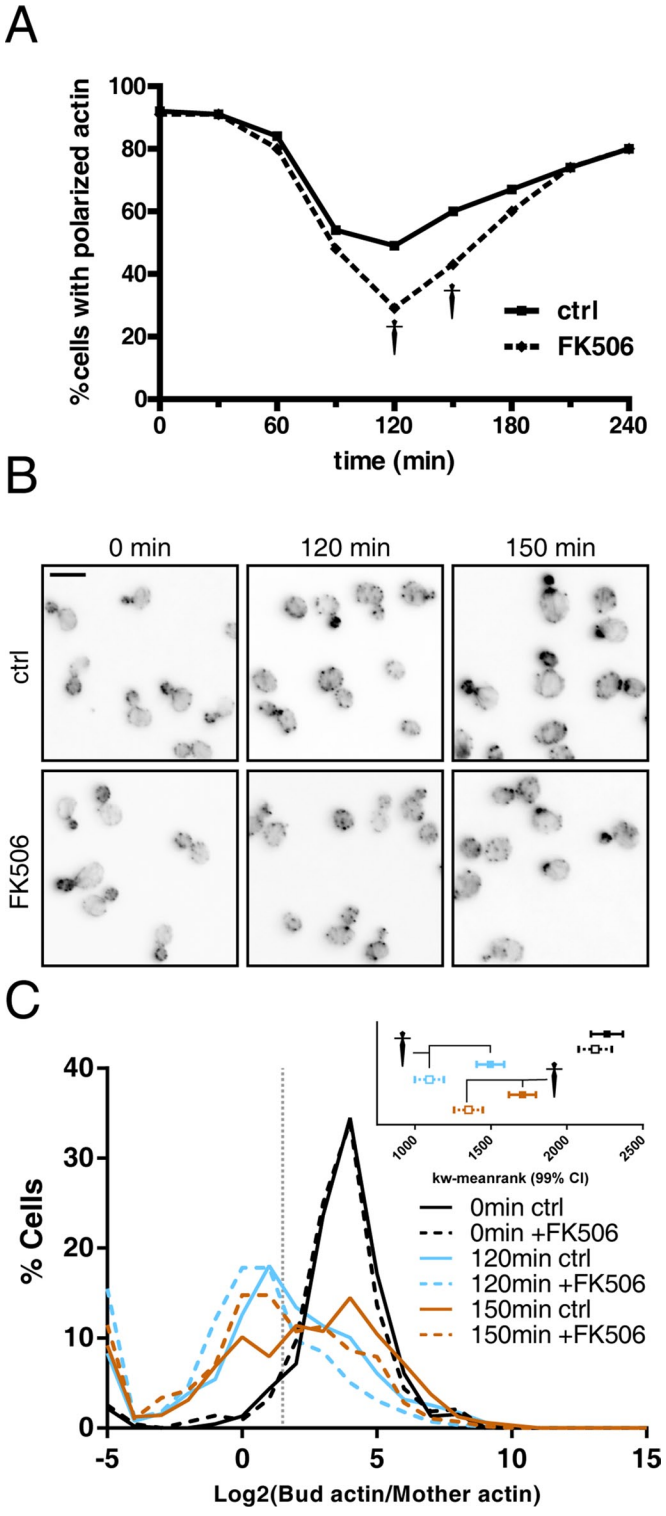

FIGURE 3: Calcineurin promotes actin repolarization during hyperosmotic stress. (A) Actin polarity during 4-h, 1.25 M KCl stress. Cells were pretreated for 30 min with 1 µg/ml FK506 or vehicle (90% EtOH/10% Tween-20), fixed at indicated time points, stained with rhodamine–phalloidin, and analyzed with CalMorph image analysis software as described in *Materials and Methods*. Cells with a bud/mother actin ratio (average fluorescence in bud)/(average fluorescence in mother cell) > 2 were scored as polarized. Data are from three independent experiments; $N > 200$ cells at each data point. $^{\dagger}p < 10^{-9}$ from statistics as described in C. (B) Representative micrographs, stained for rhodamine–phalloidin. Scale bar, 5 µm. (C) Histograms of actin polarity measurements at 0, 120, and 150 min; vertical dotted line divides polarized and depolarized cells. Inset, Kruskal–Wallis mean ranks with 99% confidence intervals. $^{\dagger}p < 10^{-9}$, Kruskal–Wallis rank sum test with Bonferroni correction.

absence of hyperosmotic stress, *inp*ΔΔΔ cells expressing high-copy *INP53* or *INP53*^{ARAQAA} grew at a rate similar to wild-type cells and, like wild-type cells, showed no change in growth rate in the presence of FK506. In contrast, *inp*ΔΔΔ cells expressing low-copy Inp53 were viable but grew slowly, indicating that synaptojanin activity was limiting. Expression of *INP53*^{ARAQAA} at low-copy resulted in even slower growth, suggesting that interaction with CN was required for full activity of Inp53. FK506 further inhibited growth of cells expressing either *INP53* or *INP53*^{ARAQAA}, and neither strain grew appreciably in the presence of 1.25 M KCl (unpublished data). These data suggest that under synaptojanin-limiting conditions, CN is required for growth and that one of its essential functions is to positively regulate Inp53.

We then examined these cells to determine whether CN promotes actin polarization by regulating Inp53. Polarization of the actin cytoskeleton was compared in *inp*ΔΔΔ cells expressing either *INP53* or *INP53*^{ARAQAA} on a low-copy plasmid (Figure 5, B and C). Under normal growth conditions, Inp53 was sufficient to polarize actin in these cells. However, inhibiting CN with FK506 resulted in actin depolarization. Furthermore, the actin cytoskeleton was depolarized in the majority of *inp*ΔΔΔ cells expressing low-copy *INP53*^{ARAQAA}, with little further depolarization when CN was inhibited with FK506 ($p < 0.0001$; Figure 5C, inset). Inp53 and Inp53^{ARAQAA} were expressed equivalently (Supplemental Figure S4). These results show that when synaptojanin activity is limiting, activation of Inp53 by CN is required to maintain a normally polarized actin cytoskeleton.

Regulation of Inp53 by calcineurin affects membrane morphology

Inp53 exerts its effects on actin polarity by dephosphorylating PI(4,5)P_2. This phospholipid is a specific component of the plasma membrane (Ooms *et al.*, 2000; Stefan *et al.*, 2002), and mutants lacking multiple synaptojanins display aberrant plasma membrane invaginations due to increased levels of PI(4,5)P_2 and a defect in synaptojanin-mediated membrane scission (Singer-Kruger *et al.*, 1998; Sun *et al.*, 2007). To determine whether regulation of Inp53 by CN affects plasma membrane morphology, we visualized the plasma membrane in *inp*ΔΔΔ cells using the PI(4,5)P_2-binding biosensor GFP-2xPH(PLCδ) (Stefan *et al.*, 2002). In contrast to the normal, smooth plasma membranes observed in *inp*ΔΔΔ cells expressing high-copy *INP53*, *inp*ΔΔΔ cells expressing a vector, and thus depleted of *INP53*, formed massive, PI(4,5)P_2-containing membrane deformations (Figure 6A). To quantify these structures, we computationally defined the membrane region of each cell using GFP-2xPH(PLCδ) intensity and counted regions that extended >10 pixels (~0.5 um) into the cytoplasm (Figure 6, A and B). Synaptojanin-limited cells expressing low-copy *INP53* had slightly more membrane invaginations per cell than the high-copy control, and inhibiting CN with FK506 exacerbated this defect. *inp*ΔΔΔ cells expressing low copy *INP53*^{ARAQAA}, which disrupts CN binding, displayed even more severe membrane deformation, which was further exacerbated by incubation with FK506. Thus analyses of both polarized actin distribution and plasma membrane morphology in cells expressing Inp53 as the sole synaptojanin revealed that CN must bind to and dephosphorylate Inp53 to achieve full synaptojanin function.

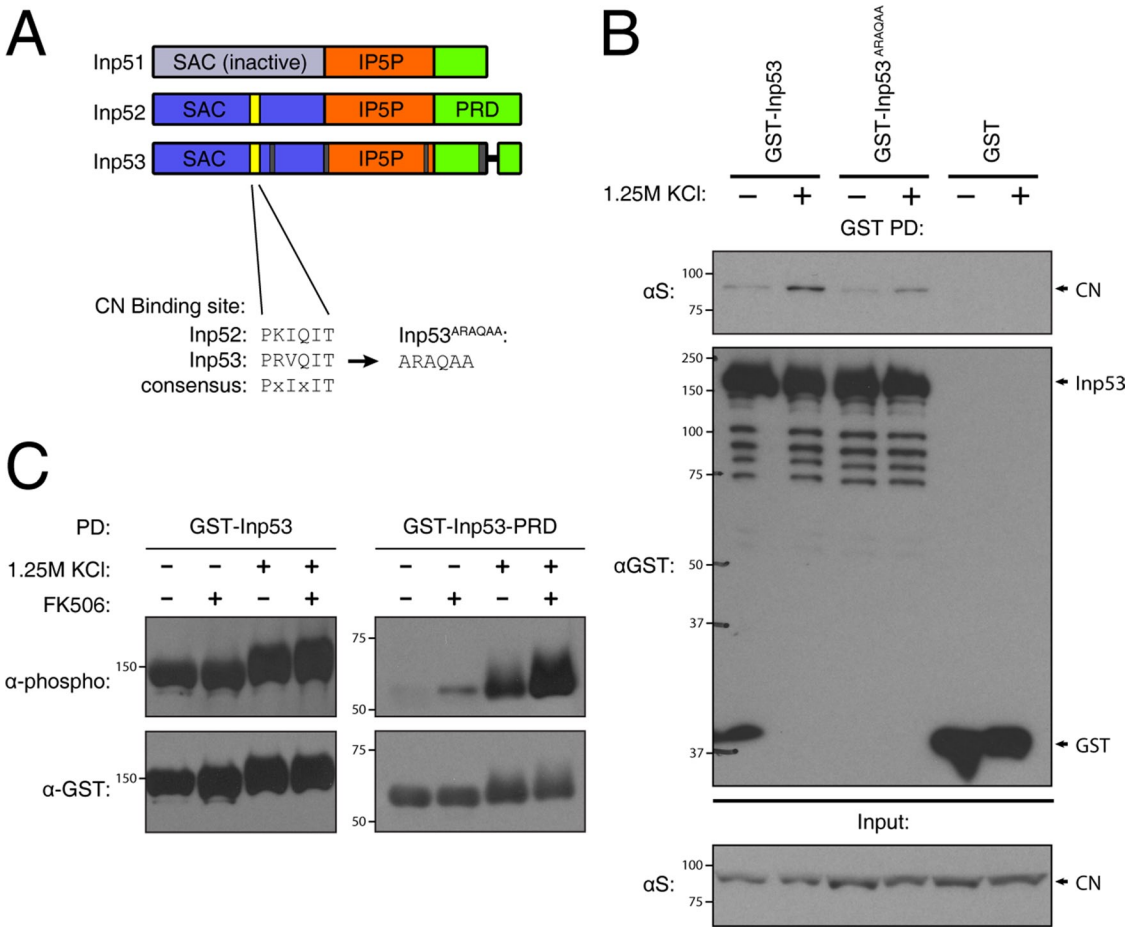

FIGURE 4: Inp53 is a calcineurin substrate. (A) Domain structure of yeast synaptojanins and creation of Inp53^{ARAQAA} allele. IP5P, inositol-polyphosphate 5-phosphatase domain; PRD, proline-rich domain; SAC, SAC1-like domain. Yellow bar, PxIxIT-CN–docking site; below, alignment with consensus. Gray bars, Inp53 peptides identified by mass spectrometry (amino acids [aa] 358–373, 523–537, 818–830, 984–1001). (B) Copurification of Cna2 with Inp53. JRY11 cells expressing GST-Inp53, GST- Inp53^{ARAQAA}, or GST alone were treated with 1.25 M KCl for 10 min where indicated and GST proteins purified with glutathione–Sepharose. Copurification of Cna2 with indicated GST-fusions was assessed by Western blotting. (C) JRY11 cells expressing GST-Inp53 or GST-Inp53(PRD)$_{aa.887-1107}$ were pretreated with 1 μg/ml FK506 or vehicle (90% EtOH/10% Tween-20) for 30 min, then treated with 1.25 M KCl for 10 min where indicated and purified as in B. Phosphorylated protein (top) and total GST-tagged protein (bottom) were assessed by Western blotting. Representative blots from more than three independent experiments are shown.

Calcineurin regulates PI(4,5)P_2 distribution in the membrane during hyperosmotic shock

In wild-type cells, CN interaction with and dephosphorylation of Inp53 is specifically stimulated during hyperosmotic stress, suggesting that CN regulates PI(4,5)P_2 pools under these conditions. Total PI(4,5)P_2 levels do not change significantly during osmotic stress (Bonangelino *et al.*, 2002), suggesting that CN-dependent activation of Inp53 may instead result in altered subcellular distribution of PI(4,5)P_2. We used the GFP-2xPH(PLCδ) biosensor to investigate PI(4,5)P_2 distribution during osmotic shock.

In unstressed WT cells, GFP-2xPH(PLCδ) was smoothly distributed throughout the plasma membrane and uniformly brighter than the adjacent cytoplasm (Figure 7A). In contrast, after a 10-min hyperosmotic shock, distribution of GFP-2xPH(PLCδ) at the membrane dramatically changed; fluorescence was confined to a few bright patches in each cell, which were separated by large regions depleted of GFP-2xPH(PLCδ), where fluorescence was not significantly higher than in the adjacent cytoplasm (Figure 7A). This change in GFP-2xPH(PLCδ) distribution was quantified by determining the percentage of total membrane area in each cell that displayed significant enrichment of GFP-2xPH(PLCδ) fluorescence relative to the adjacent cytoplasm (Figure 7B; see *Materials and Methods*). This analysis captured the uniform, bright GFP-2xPH(PLCδ) localization in unstressed cells: on average, >70% of the membrane showed enriched GFP-2xPH(PLCδ) fluorescence. In contrast, after hyperosmotic shock, only 17% of the membrane, on average, showed enriched GFP-2xPH(PLCδ) (Figure 7; $p < 0.0001$). These results document a major redistribution of PI(4,5)P_2 into enriched and depleted membrane domains during osmotic shock, which may also underlie changes in membrane morphology previously described by electron microscopy (Dupont *et al.*, 2010).

The extent of GFP-2xPH(PLCδ) depletion during osmotic shock also depended on CN: when CN was inhibited, 24% of the membrane retained enriched GFP-2xPH(PLCδ), a significantly greater area than in control cells (Figure 7, A–C; $p < 0.0001$). This result is consistent with CN-dependent activation of Inp53 during osmotic shock enhancing the depletion of PI(4,5)P_2 from large regions of the membrane and likely represents an important mechanism by which the cells adjust to the membrane stress induced by rapid volume loss.

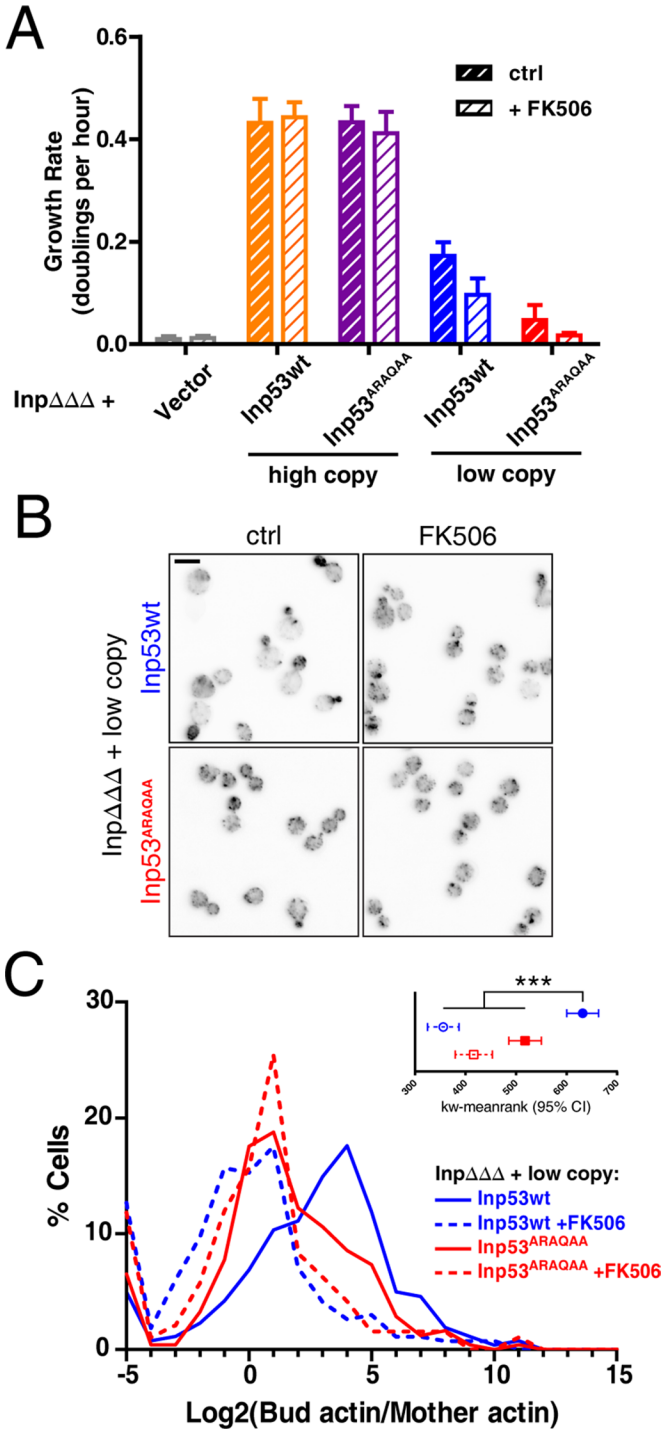

FIGURE 5: Calcineurin regulates actin polarity via Inp53. (A) Inp53 growth rate (doublings per hour) during exponential growth in dextrose. (B) Representative micrographs of *inp*ΔΔΔ cells expressing low-copy *INP53* or *INP53*^{ARAQAA} stained with rhodamine–phalloidin. (C) Histograms of actin polarity measurements in *inp*ΔΔΔ cells expressing low-copy *INP53* or *INP53*^{ARAQAA} (pRS316-*INP53* and pRS316- *INP53*^{ARAQAA}) in dextrose without stress. N > 200 cells/condition; insets are Kruskal–Wallis mean ranks with 95% confidence interval; ***$p < 0.0001$.

Molecular mechanisms of Inp53 regulation by calcineurin

The phenotypic effects of the CN-binding deficient Inp53^{ARAQAA} mutant and of CN inhibition suggest that in vivo, CN acts to activate Inp53. We next investigated whether CN activates Inp53 by altering its intrinsic catalytic activity or by regulating its interactions with other proteins.

To examine whether hyperphosphorylation induced by hyperosmotic stress or dephosphorylation by CN directly altered Inp53 catalytic activity, we purified Inp53 from yeast under conditions that maintained its phosphorylation state and SAC and IP5Pase domain activities (Figure 8A; Guo *et al.*, 1999) and analyzed the kinetics of PI(4,5)P_2 dephosphorylation by Inp53 in vitro. GST-Inp53 and GST were purified from cells treated either with vehicle or FK506 and grown in the presence or absence of hypertonic shock. GST-Inp53, but not GST, exhibited PI(4,5)P_2 phosphatase activity in vitro (Figure 8B and Supplemental Figure S5) which was statistically equivalent in all preparations tested (Figure 8B). Thus we find no evidence that the intrinsic catalytic activity of Inp53 is altered either by the massive hyperphosphorylation that occurs after osmotic shock or by subsequent dephosphorylation via CN. However, changes in PI(4,5)P_2 distribution in the membrane suggest that sites of Inp53 action are reorganized.

Therefore we tested whether any of the established or predicted protein–protein interactions for Inp53 were altered by hyperosmotic shock or its regulation by CN. In unstressed cells, Inp53 functions primarily to regulate phosphoinositide-dependent sorting of proteins at the TGN and interacts directly with clathrin via an LLDID motif in the Inp53-PRD (Ha *et al.*, 2001, 2003; Daboussi *et al.*, 2012). Equivalent amounts of clathrin heavy chain (Chc1) copurified with Inp53 and Inp53^{ARAQAA}, but copurification of Chc1 with both proteins decreased after hyperosmotic shock (Figure 9A). Hyperphosphorylation of the Inp53-PRD may be responsible for reduced clathrin binding; we identified numerous phosphorylation sites in the Inp53-PRD that increased during osmotic stress, including S_{914}, which immediately precedes $LLDID_{915\text{-}919}$ (unpublished data). Loss of interaction with clathrin may indicate a repurposing of Inp53 from its normal role at the TGN to a function at actin patches and is consistent with reports of Inp53 translocation to actin patches during hyperosmotic shock (Ooms *et al.*, 2000).

We next investigated whether Inp53 interacts with actin patch/endocytic proteins. Like synaptojanins Inp52 and Inp53, Rvs167, a yeast homologue of amphiphysin/endophilin, promotes repolarization of the actin cytoskeleton during hyperosmotic stress, and *rvs167* mutants are sensitive to hyperosmotic stress (Bauer *et al.*, 1993). Inp53 and Rvs167 show genetic interactions (Aguilar *et al.*, 2010), but no physical interaction between either Inp52 or Inp53 and Rvs167 has been reported. We found that Rvs167-GFP copurified equivalently with both GST-Inp53 and GST-Inp53^{ARAQAA} (Figure 9B). There was no significant change in Rvs167-Inp53 association under hyperosmotic conditions, but Rvs167 showed slower electrophoretic mobility during hyperosmotic stress, suggesting that it may be phosphorylated or otherwise modified under these conditions.

Inp53 was previously reported to interact with the actin patch components Bsp1, Bzz1, and Sla1 in yeast two-hybrid analyses (Wicky *et al.*, 2003; Tonikian *et al.*, 2009). Bzz1 and Sla1 both contain SH3 domains that are predicted to interact with the Inp53-PRD (Tonikian *et al.*, 2009). Bsp1 is an endocytic protein of unclear function that binds the SAC domain of Inp52 and Inp53 and arrives late during internalization at endocytic sites along with other components of the actin module (Wicky *et al.*, 2003; Tonikian *et al.*, 2009). Bzz1/syndapin stimulates Las17/WASP-mediated actin polymerization and recognizes shallow membrane curvature through its F-BAR domain. We were unable to detect either Bsp1 or Bzz1 copurification with Inp53 in unstressed cells but saw substantial copurification of both proteins with Inp53 during hyperosmotic

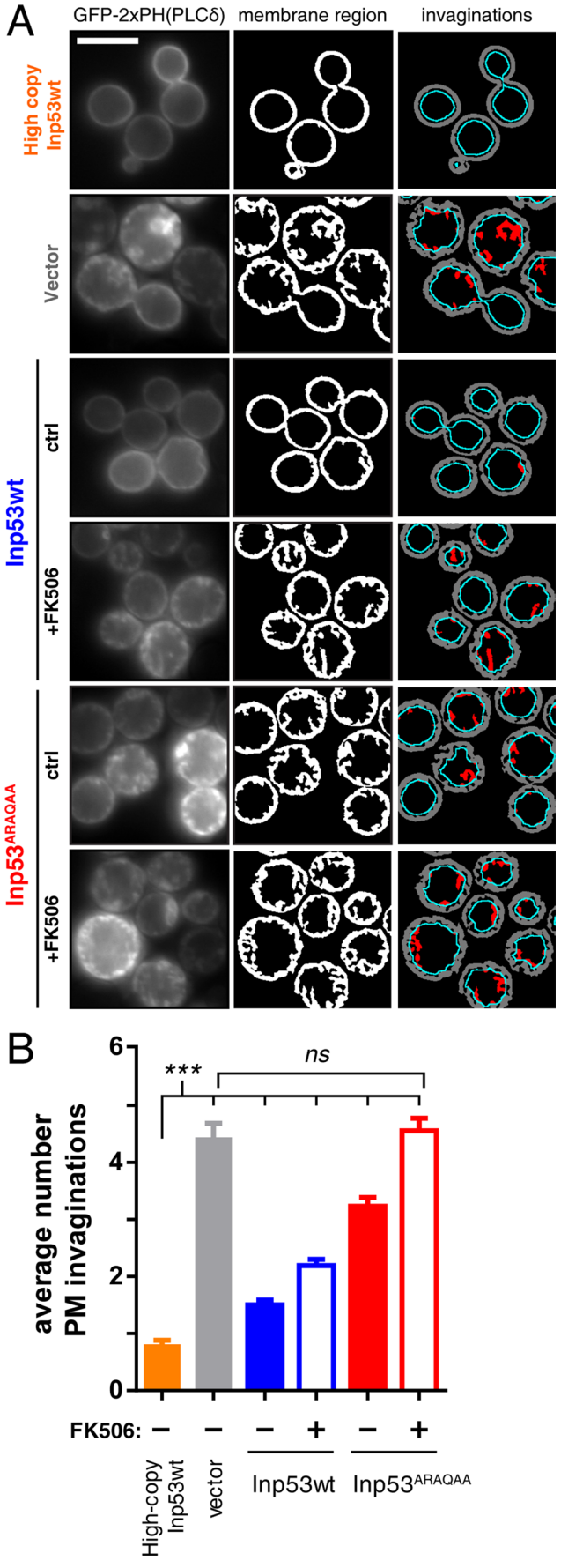

shock (Figure 9, C and D); neither the Inp53-Bsp1 nor the Inp53-Bzz1 interaction was substantially altered by disruption of the CN binding site in Inp53^{ARAQAA} (Figure 9, C and D). Bzz1 levels did not change during hyperosmotic shock, suggesting that its ability to interact with Inp53 was enhanced during stress. By contrast, the amount of Bsp1 in the soluble fraction of our extracts changed dramatically. Under all conditions, the majority of Bsp1 was present in the insoluble pellet fraction. However, the soluble pool of Bsp1 increased significantly in extracts of cells exposed to hyperosmotic stress, which may explain its copurification with Inp53 under these conditions (Figure 9C). Thus interaction of Inp53 with both Bsp1 and Bzz1 occurs specifically during osmotic shock.

Finally, we found that Inp53 interacts with the endocytic coat protein Sla1/intersectin. Sla1 has diverse functions during endocytosis, including roles in cargo recognition, where it binds the NPFXD motif; as a regulator of the actin nucleation-promoting factor Las17/WASP; and as a clathrin-binding adaptor (Mahadev *et al.*, 2007; Piao *et al.*, 2007; Feliciano and Di Pietro, 2012). Inp53 copurified with Sla1/intersectin in unstressed cells, and this interaction was substantially enhanced during hyperosmotic stress. By contrast, the CN-binding–deficient Inp53^{ARAQAA} copurified with the same low amount of Sla1 when purified from either stressed or unstressed cells (Figure 9E). Thus the Inp53-Sla1 interaction is enhanced during hyperosmotic stress, and this effect is dependent on CN. Despite the prediction that SH3 domains in both Bzz1 and Sla1 should bind to proline-rich motifs in the Inp53-PRD, the Inp53-PRD alone was insufficient to copurify either Bzz1 or Sla1 (Supplemental Figure S6). Instead, interactions between Inp53, Sla1, and CN likely occur in part of a larger complex. Consistent with this idea, Sla1 contains numerous phosphorylation sites that are regulated by CN in vivo but lacks a predicted CN docking motif (Goldman *et al.*, 2014). Thus, after hypertonic shock, Inp53 may form a complex with both Sla1 and CN that facilitates Sla1 and Inp53 dephosphorylation.

DISCUSSION

Membrane structure must be restored in response to hyperosmotic shock

Hyperosmotic shock causes dramatic changes throughout the cell and requires a broad response coordinated by multiple signaling pathways. At the center of this response, the HOG pathway acts to restore turgor pressure and control gene expression (Saito and Posas, 2012). Independently, the cell wall sensor Wsc1 promotes depolarization of the actin cytoskeleton (Balguerie *et al.*, 2002) and induces a widespread secretory arrest (Nanduri and Tartakoff, 2001a,b); depolymerization of actin cables liberates monomeric

FIGURE 6: Calcineurin regulates membrane morphology via Inp53. (A) Representative images of *inp*ΔΔΔ (LSY312) cells expressing GFP-2xPH(PLCδ) and high-copy *INP53* (pRS426-*INP53*), vector only (pRS316), or low-copy *INP53* or *INP53*^{ARAQAA} (pRS316-*INP53* or pRS316-*INP53*^{ARAQAA}) were grown in dextrose, then treated with 1 μg/ml FK506 or vehicle for 2 h where indicated. Middle, membrane trace of GFP-2xPH(PLCδ) identified computationally (see *Materials and Methods*). Right, based on the computationally identified membrane region, we counted invaginations (marked in red) that extend further than 10 pixels (~0.5 μm) into the cell (blue line). Scale bar, 5 μm. (B) Average number of large (0.5 μm) invaginations quantified from GFP-2xPH(PLCδ) membrane traces such as those shown in A. Error bars are SEM. ***$p < 0.0001$ for all pairwise comparisons except where marked; *n.s*, not significant; one-way ANOVA with Tukey's correction for multiple comparisons.

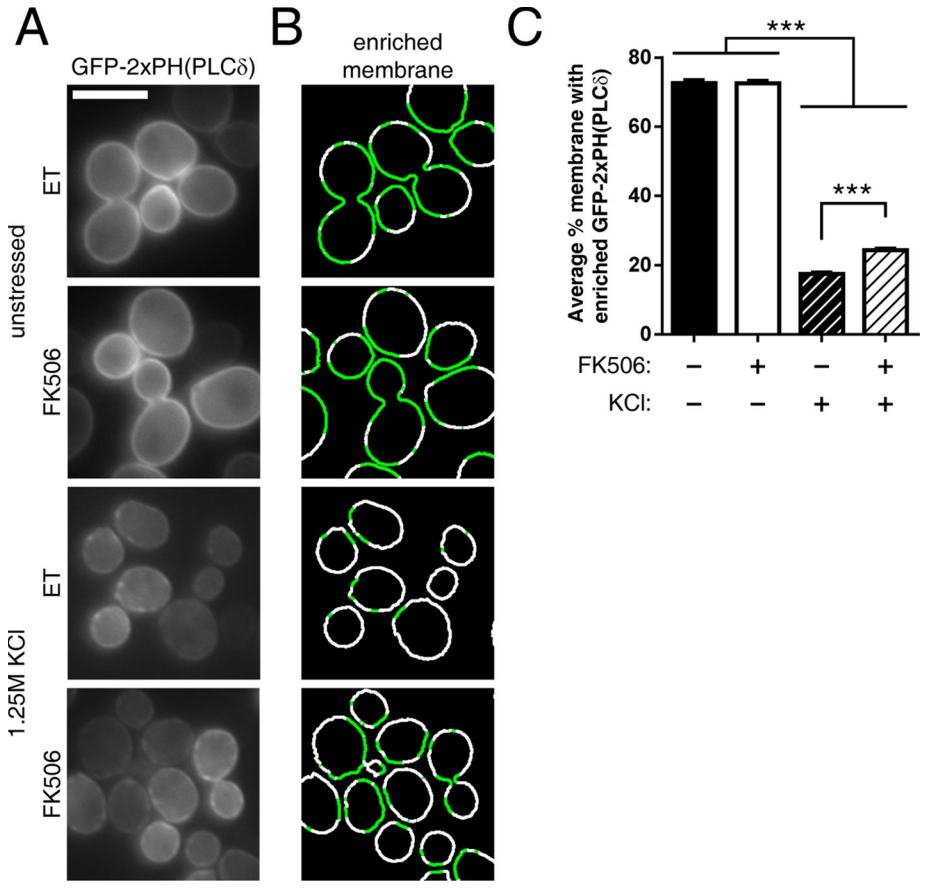

FIGURE 7: Calcineurin regulates PI(4,5)P_2 distribution during osmotic shock. (A) Representative images of wild-type (BY4741) cells expressing GFP-2xPH(PLCδ). Cells were treated with 1 μg/ml FK506 or vehicle for 30 min; osmotic shock was induced with 1.25 M KCl for 10 min where indicated. (B) Membrane regions with >10% enriched GFP-2xPH(PLCδ) compared with adjacent cytoplasm are marked in green; see *Materials and Methods*. (C) The percentage of total membrane in each cell that was enriched for GFP-2xPH(PLCδ) was averaged and plotted. Error bars represent SEM. ***$p < 0.0001$; one-way ANOVA and Tukey's multiple comparison posttest. For each condition, $N > 700$ cells, from four independent experiments.

actin, which stimulates Ssk2 to activate the polarisome (Yuzyuk, 2002, 2003). We show here that the Ca^{2+}/calmodulin–dependent phosphatase CN also functions during osmotic stress, which was not previously appreciated.

Hypertonic shock induces distinct physiological responses, depending on its severity. As osmotic challenge increases to ~500 mM KCl, loss of cell volume is mild because turgor pressure is only partially depleted. Over this range, the HOG pathway becomes increasingly active to restore and maintain turgor pressure (Schaber *et al.*, 2010; Saito and Posas, 2012; Lee *et al.*, 2013). More intense osmotic stress leads to complete loss of turgor, and for increasing osmotic challenge beyond this point, volume loss is extreme. Dramatic cell shrinkage confines the plasma membrane to a much-reduced surface area, causing deep invaginations to form (Dupont *et al.*, 2010) and presenting an acute challenge that must be resolved rapidly and with precise spatial control.

Ca^{2+} signaling is well suited to regulate such responses. Hyperosmotic shock triggers a rapid and transient Ca^{2+} signal (Denis and Cyert, 2002) and promotes an immediate redistribution of CN, mediating its interaction with specific targets, such as Inp53. Similarly, the uniform distribution of PI(4,5)P_2 in the membrane quickly changes into a mosaic of depleted and PI(4,5)P_2–enriched domains, which CN regulates, potentially through Inp53. These PI(4,5)P_2 patches are well suited, by binding and activating a host of known effector proteins, to pattern the localized events required to restore the integrity of the cell surface.

New insights into CN signaling specificity in *S. cerevisiae*

A diverse array of >40 proteins involved in polarized growth, cell cycle regulation, mating, autophagy, and many other cellular processes have been identified as CN targets (Goldman *et al.*, 2014). Where and when these proteins are regulated by CN have yet to be elucidated. We show here that CN undergoes major localization changes during hyperosmotic shock, which may restrict the substrates it dephosphorylates. In particular, we find that CN colocalizes with a subset of actin patches, perhaps indicating transient localization to sites of endocytosis, and binds preferentially to Inp53 during hyperosmotic shock. In contrast, activation of the CN-dependent Crz1 transcription factor is blocked (Figure 10A). Intense osmotic shock delays multiple signaling events, including Crz1 nuclear translocation, possibly because of impaired diffusion caused by water loss (Miermont *et al.*, 2013). However, changing CN's binding partners also affects downstream signaling; artificially strengthening the CN-Crz1 interaction, for example, causes growth defects by blocking the interaction of CN with other substrates (Roy *et al.*, 2007). Therefore CN signaling outcomes during hyperosmotic stress are likely specified by its subcellular distribution and protein–protein interactions, in agreement with important roles for CN localization in other fungi and in mammals (Oliveria *et al.*, 2007; Juvvadi *et al.*, 2011; Kozubowski *et al.*, 2011). The mechanism(s) responsible for the CN localization changes caused by hyperosmotic stress are unknown, as significant colocalization of CN and Inp53 was not observed (Supplemental Figure S2, B and C). However, similar approaches to those described here will likely identify additional scaffold candidates. We also suggest that interactions between Inp53 and CN during hyperosmotic stress bring CN into proximity with substrates like Bsp1 and Sla1 that lack canonical docking motifs but show CN-dependent dephosphorylation (Goldman *et al.*, 2014). Thus hyperosmotic shock illustrates how a specific environmental condition can tune CN signaling by modifying localization and substrate access.

Regulation of endocytosis during hyperosmotic shock

This study provides some initial insights into molecular events that occur at depolarized actin patches in cells responding to intense osmotic shock. Endocytosis is regulated by a densely interconnected network of proteins (Johnson and Hummer, 2013). During osmotic stress, we show that components of this network are dephosphorylated by CN and are also antagonistically hyperphosphorylated. Key interactions between Inp53 and other proteins involved in scission and actin force generation (Sla1 and Bzz1) are altered, and the interaction of Inp53 with clathrin is reduced, presumably

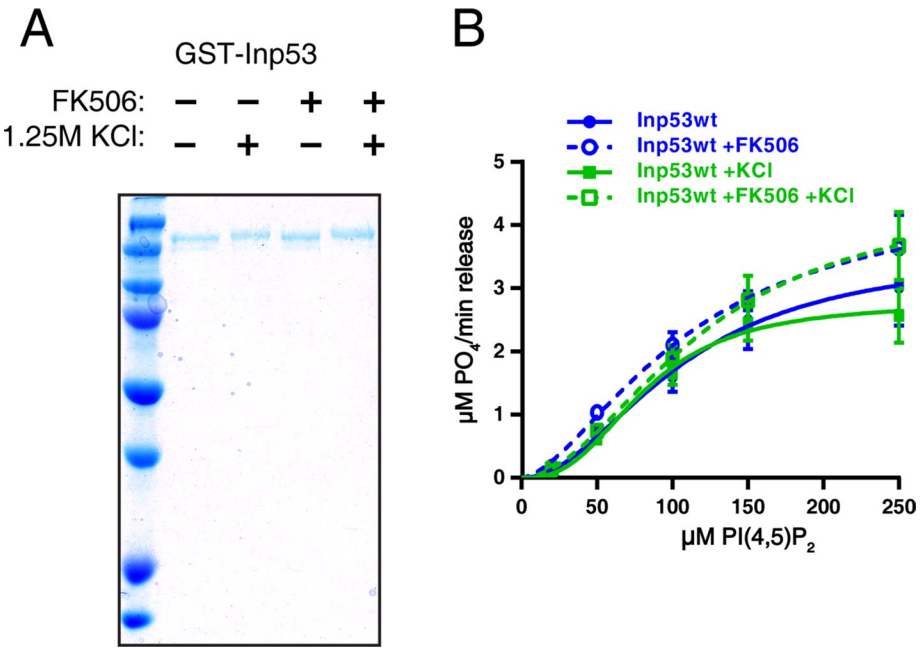

FIGURE 8: Calcineurin and hyperosmotic stress do not affect Inp53 catalytic activity. (A) Coomassie-stained GST-Inp53 purified from cells treated with 1 μg/ml FK506 or vehicle and with or without 10 min of 1.25 M KCl. (B) The in vitro activity of each GST-Inp53 preparation shown in A was determined; the initial reaction rate is plotted as a function of $PI(4,5)P_2$ concentration. GST purified equivalently displayed no phosphatase activity (Supplemental Figure S5).

directing it away from the TGN (Figure 10B). This stress-specific remodeling may adjust the endocytic machinery to the unique physiological circumstances that accompany intense hypertonic stress. For example, loss of turgor reduces the requirement for actin-generated force during endocytosis (Aghamohammadzadeh and Ayscough, 2009), and the deep membrane invaginations observed after intense osmotic stress suggest that a large amount of membrane may need to be internalized. Although the mechanisms by which osmotically stressed yeast resolve these invaginations have not been elucidated, they may be similar to the process of ADBE, which has been well studied in neurons.

During periods of intense stimulation, massive release of synaptic vesicles deposits a large amount of membrane at the cell surface (Meunier *et al.*, 2012; Kittelmann *et al.*, 2013), which cannot be efficiently retrieved by CME. Instead, ADBE is induced to pinch off large membrane invaginations, forming endosome-like compartments (Cousin, 2009; Saheki and De Camilli, 2012). ADBE is activated by Ca^{2+}/CN (Evans and Cousin, 2007) and may be physiologically similar to the CN-dependent processes that are required to maintain yeast viability after intense hypertonic shock.

To carry out ADBE, the cell repurposes many of the same components that participate in CME, that is, synaptojanin, endophilin, syndapin, dynamin, and intersectin (Mani *et al.*, 2007; Clayton *et al.*, 2009; Winther *et al.*, 2013). CN initiates ADBE by dephosphorylating synaptojanin, dynamin, and other proteins collectively termed the dephosphins. Dephosphorylation promotes synaptojanin–endophilin and dynamin–syndapin binding (Mani *et al.*, 2007; Clayton *et al.*, 2009). Both of these interactions occur and are specifically required only during ADBE (Figure 9C). In particular, syndapin, which contains an F-BAR domain, stabilizes shallow membrane curvature and may facilitate formation and/or resolution of the large membrane invaginations unique to ADBE. In addition, Cdk5 kinase and CN phosphatase activity are simultaneously required during ADBE (Evans and Cousin, 2007). Similarly, we observe both hyperphosphorylation and CN-mediated dephosphorylation of the Inp53-PRD during hypertonic shock, suggesting that coordination between CN and antagonistic kinases may be required to temporally or spatially regulate the activity of Inp53. Thus the parallel recruitment/interaction with the homologous yeast proteins Inp53 (synaptojanin), Rvs167 (amphiphysin/endophilin), Bzz1 (syndapin), Sla1 (intersectin) and CN during hyperosmotic shock suggest that this yeast response is strikingly similar to ADBE at the molecular level.

Although CN is well conserved between yeast and humans, with 44% sequence identity (Cyert *et al.*, 1991), its functions and substrates have significantly diverged. Among >70 CN targets, synaptojanin/Inp53 is one of only two proteins identified as CN substrates in both yeast and mammals (Goldman *et al.*, 2014). Thus regulation of synaptojanin may be one of CN's primordial functions, and we hypothesize that the activation of Ca^{2+}/CN and $PI(4,5)P_2$ signaling to regulate endocytosis is a fundamental and conserved response to excess membrane in eukaryotic cells.

MATERIALS AND METHODS

Growth media and general methods

Yeast media and culture conditions were essentially as previously described, except that twice the levels of amino acids and nucleotides were used in synthetic complete medium (Sherman, 1991). Yeast transformations were carried out by the lithium acetate method (Ausubel *et al.*, 1991). For 4x-CDRE-*lacZ* reporter assays, cells were grown to mid log phase, and $CaCl_2$ or KCl was added for 2 h as noted. β-Galactosidase activity was measured as previously described (Bultynck *et al.*, 2006). Values represent an average of three independent extracts, each measured in triplicate. Error bars indicate the SD. Yeast strains are listed in Supplemental Table S1a; strains from the yeast deletion collection were purchased from Open Biosystems (Huntsville, AL). Plasmids used in this study are listed in Supplemental Table S1b. FK506 was used from a 10 mg/ml stock dissolved in 9:1 EtOH/Tween-20 and used at 1 μg/ml (LC Laboratories, Woburn MA).

Yeast strain construction

YEG1 was created from YMJ38 (provided by Maria Molina, Universidad Complutense, Madrid, Spain) by transformation with the pCNA1::URA3hisG deletion cassette and counterselected on 5-fluoroorotic acid to restore URA-. YEG2 was created from YEG1 by transforming with the S-TEV-ZZ-URA3 cassette from pKW953, PCR amplified with Vent DNA Polymerase (New England BioLabs, Ipswich, MA) and primers 5′-GGCAGAAAGTACATGAACATGATGCAAAGAATGATAGCAAAGCAGGTCGACG GATCCCCGGG-3′ and 5′-CTTACTTATTGAAGTATGTACAGTGGAAATAGGAGCTTTCTGAATTCGAGCTCGTTTTCGA-3′. YEG3 and YEG4 were created from BY4741 by transformation with pEG4 or pEG5 linearized with *Nde*I. Tagged CN proteins (YEG2, Cna2-S-Tev-ZZ, YEG3, Cna1-3GFP, YEG4, and Cna2-3GFP were functional; Goldman *et al.*, 2014; unpublished data). YEG6, YEG7, and YEG8 were created by transformation of

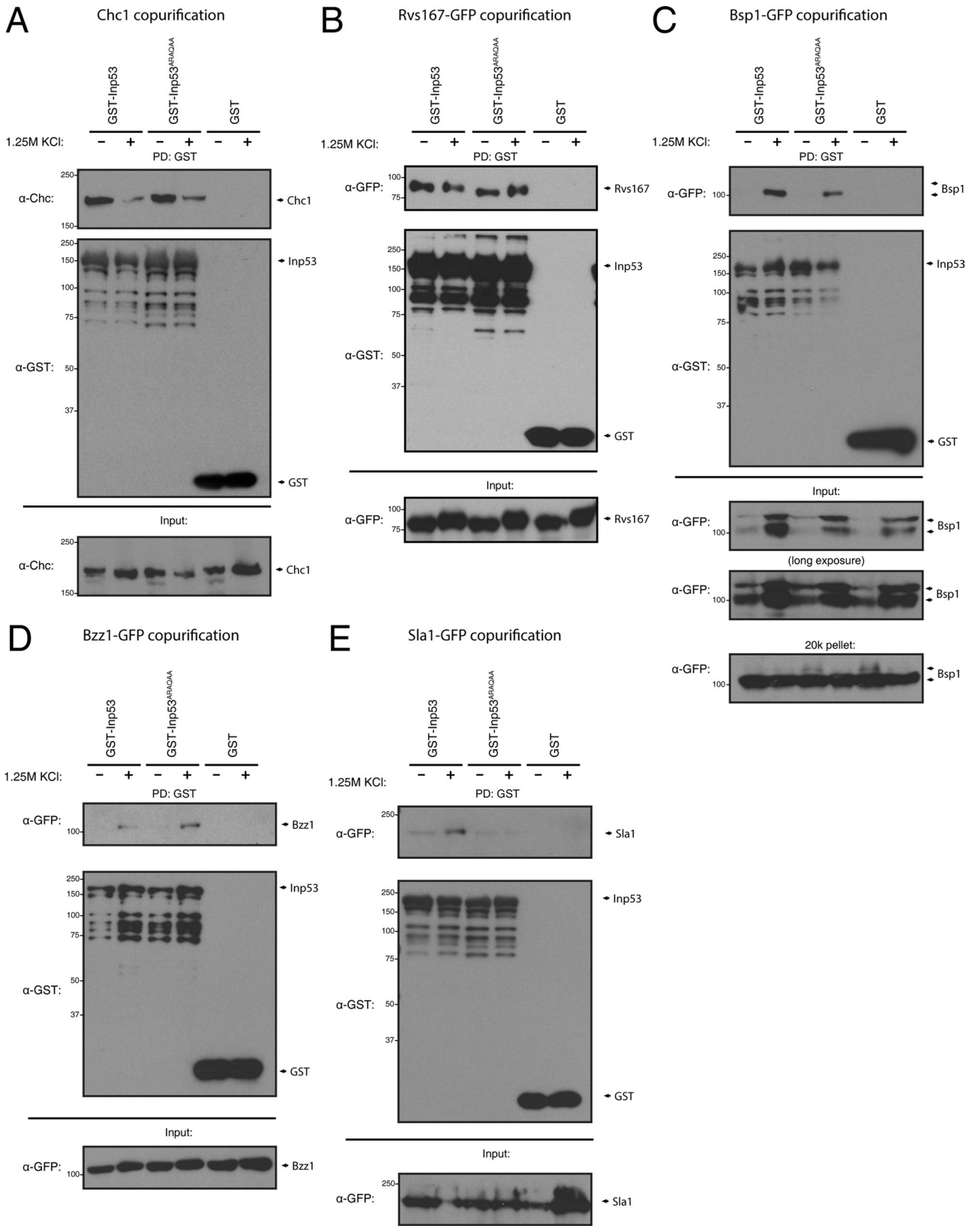

FIGURE 9: Molecular mechanism of Inp53 regulation by calcineurin. Wild-type cells (A) or cells expressing the indicated GFP fusion from endogenous loci (B–E) and expressing GST-Inp53, GST-Inp53 ^{ARAQAA}, or GST were treated with or without 1.25 M KCl for 10 min, and GST- tagged proteins were purified with glutathione-Sepharose. (C) Soluble (Input) and insoluble fractions (20,000 × *g* pellet). Copurification of the GFP fusion proteins with indicated GST-fusions was assessed by Western blotting; representative blots from more than three independent experiments are shown.

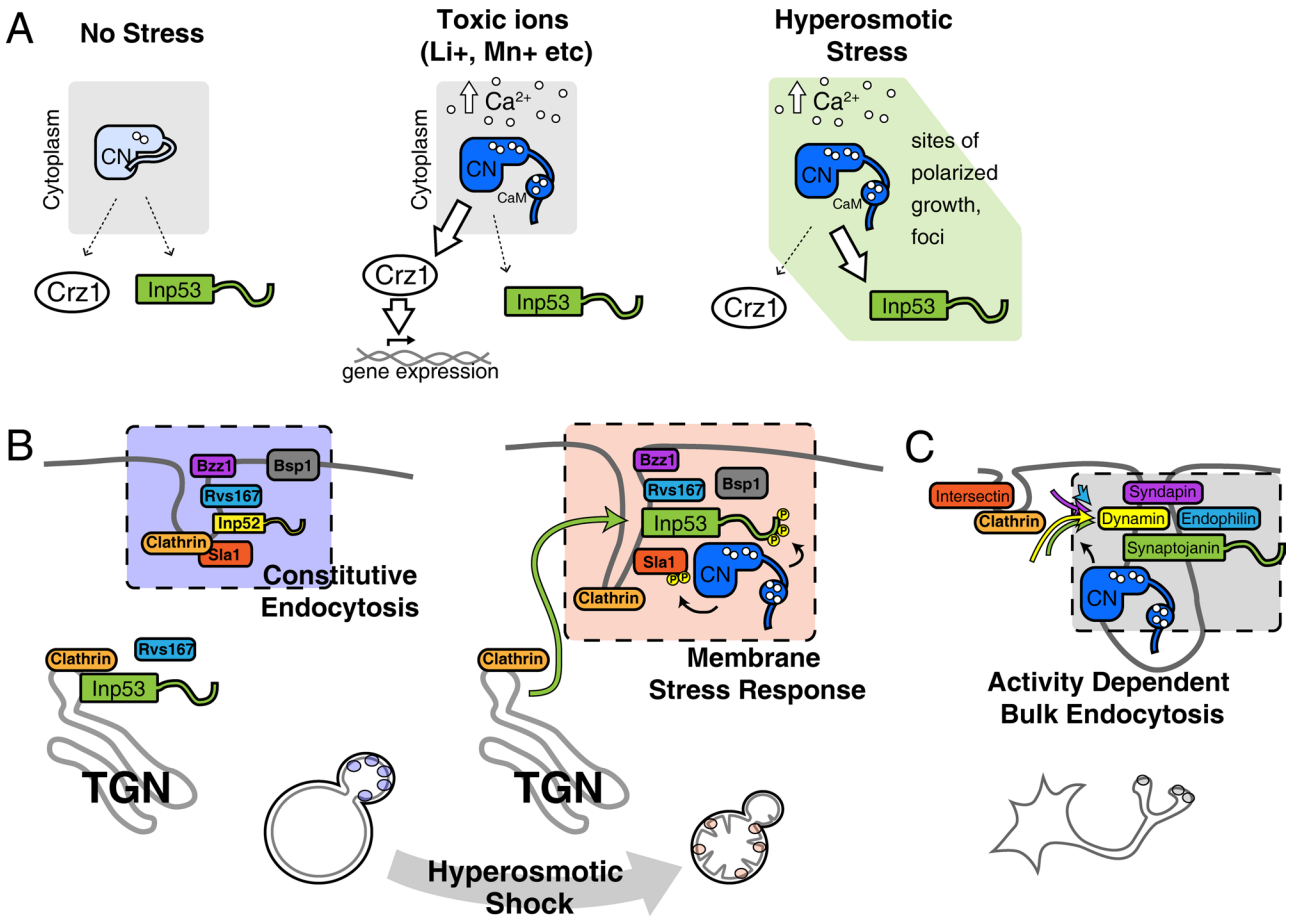

FIGURE 10: Model. (A) CN is inactive in unstressed cells, and in response to many stress conditions, remains cytoplasmic and is activated by Ca^{2+}/calmodulin, promoting dephosphorylation of Crz1 and resulting in gene expression. In response to hyperosmotic shock, CN relocalization promotes activation of Inp53 but blocks Crz1 dependent transcription. (B) In unstressed cells, constitutive endocytosis is polarized and occurs with the involvement of clathrin, Sla1, Inp52, Rvs167, Bzz1, Bsp1, and many other proteins not shown; Inp53 associates with clathrin and Rvs167 and functions primarily at the TGN. During hyperosmotic shock, the composition of actin patches changes, with Inp53 losing interactions with clathrin and gaining interactions with Sla1, Bzz1, Bsp1, and CN; Inp53 also becomes hyperphosphorylated, and CN dephosphorylates it and Sla1. (C) Many endocytic proteins and their interactions are conserved in mammals, where CN promotes association between synaptojanin, dynamin, amphiphysin, syndapin, and intersectin during synaptic vesicle endocytosis.

BY4741 with *Nde*1-linearized pEG4 and with *Xba*I-linearized pEG38 or *Bsu*36I-linearized pEG27 or pEG28, respectively.

Plasmid construction

A C-terminal fragment of *CNA1* was amplified with primers 5′-CCCGCTCGAGCAGTGCGCCAAACTACCTGGAC-3′ and 5′-CGCGGATCCTCCAGTTGTGGC TTTTTCTCCGCTCCC-3′ and inserted as a *Xho*I/*Bam*HI fragment into pB1963 to create pCNA1-3GFP. A C-terminal fragment of *CNA2* was amplified with primers 5′-CCCGCTCGAGGGGAGATTCCCTCTCATGGC-CTG-3′ and 5′-CGCGGATCCTCTTTGCTATCATTCTTTGCATC-ATGTTCATG-3′ and inserted as a *Xho*I/*Bam*HI fragment into pB1963 to create pCNA2-3GFP.

Inp53 was amplified with primers 5′- GCTCTAGACATGAT-TATCTTTGTTTCAGAAGAACCTGAAAG-3′ and 5′-ACGCGTCGAC-TCATTTTGGGGTCAATGGCTGCC-3′ from genomic DNA and ligated in- frame into pEG(KT) as an *Xba*I/*Sal*I fragment to create pEG6(GST-Inp53). Inp53 SAC domain was amplified with primers 5′-GCTCTAGACATGATTATCTTTGTTTCAGAAGAACCTGAAAG-3′ and 5′-ACGCGTCGACTCATCCCAACAAAGTATCGATATTTTGTT-GCTTTTC-3′ and ligated in- frame into pEG(KT) as an *Xba*I/*Sal*I fragment to create pEG7. The Inp53 IP5P domain was amplified with primers 5′-GCTCTAGACAGGTTACCGTATCAGAAAGCAG-TGC-3′ and 5′-ACGCGTCGACTCATTCTTCGGGATGCTCTTGTTT-GTATTC-3′ and ligated in-frame into pEG(KT) as an *Xba*I/*Sal*I fragment to create pEG8. The Inp53 PRD domain was amplified with primers 5′-GCTCTAGACCCGGGTTCTCTGATATCGGATCTTC-3′ and 5′-ACGCGTCGACTCATTTTGGGGTCAATGGCTGCC-3′ and ligated in frame into pEG(KT) as an *Xba*I/*Sal*I fragment to create pEG9.

pEG12 was created using PCR mutagenesis from pGST-Inp53 with internal primers 5′-GGGAGCAAGGTACCTCTTTAATCAAT-GCTAGAGCACAAGCAGCCAGATCATTTGAAGCCACCCA-ACCG-3′ and 5′-CGGTTGGGTGGCTTCAAATGATCTGGCTGCTT-GTGCTCTAGCATTGATTAAAGAGGTACCTTGCTCCC-3′ and outside primers 5′-GCAGATCTATGATTATCTTTGTTTCAGAAGAAC-CTGAAAGG-3′ and 5′-ACGCGTCGACTCACCGGCCGAGCAAAG-TATCGATATTTTGTTGCTTTTCTTTATCC-3′ and inserted into pEG(KT) cut with *Bam*HI/*Sal*I as a *Bgl*II/*Sal*I fragment; pEG12 was then cut with *Eag*I/*Sal*I, and *Eag*I/*Bam*HI and *Bam*HI/*Sal*I fragments of Inp53(IP5P) and Inp53(PRD) amplified from pEG6 template with

primers 5′-GCAGATCTCTCGGCCGGTTACCGTATCAGAAAGCAGTGCAAC-3′ and 5′-ACGCGTCGACTCAGGATCCTGGTTCTTCGGGATGCTCTTGTTTGTATTCTG-3′, and primers 5′-GCAGATCTCCAGGATCCCTGATATCGGATCTTCTCAGCC-3′ and 5′-ACGCGTCGACTCATTTTGGGGTCAATGGCTGCC-3′, respectively, were inserted to create pEG11(GST-Inp53ΔCN). A *Bsa*BI/*Hin*dIII fragment from pEG11(GST-Inp53ΔCN) was subcloned into pRS426-Inp53 and pRS316-Inp53 to create pRS426-Inp53ΔCN and pRS316-Inp53ΔCN, respectively. pRS426GFP-2xPH(PLCδ) was converted from URA3 to ADE2 by gap repair, yielding pEG30. mKate was amplified (Shcherbo *et al.*, 2007) with primers 5′-CGTTGAATTCGCATGCTACCCATACGATGTTCCAGATTACGCTATGGTGAGCGAGCTGATTAAGG-3′ and 5′-CGCGTTAGGGCCCGATATCGAATTCTCATCTGTGCC-3′ and inserted into pRS303 as a *Eco*RI-*Apa*1 fragment. 3xmKate was amplified with 5′-CGTTGAATTCGCATGCTACCCATACGATGTTCCAGATTACGCTATGGTGAGCGAGCTGATTAAGG-3′, 5′-CGTAAAGCTTTCTGTGCCCCAGTTTGCTAG-3′, 5′-CGTAAAGCTTGGAGCAATGGTGAGCGAGCTGATTAAGG-3′, 5′-CGTACTCGAGTCTGTGCCCCAGTTTGCTAG-3′, 5′-CGTACTCGAGGGAGCTATGGTGAGCGAGCTGATTAAGG-3′, and 5′-CGCGTTAGGGCCCGATATCGAATTCTCATCTGTGCC-3′ and inserted as *Eco*RI-*Hin*dIII, *Hin*dIII-*Xho*I, and *Xho*I-*Apa*I fragments into pRS303. Inp53 and Inp53^{ARAQAA} C-terminal fragments (amino acids 203–1107) were amplified with 5′-GTCTAGtctagaGGTTAATGGCCTGCTGTTTGTTGG-3′ and 5′-GCCGCATGCTTTTGGGGTCAATGGCTGCC-3′ and inserted as an *Xba*I-*Sph*I fragment into pRS303-3xmKate. Abp1 C-term was amplified with 5′-GGTGTAGAGCTCAGGATTGGCCGCTTCAGAAAAAGAGG-3′ and 5′-CCACATGAATTCGTTGCCCAAAGACACATAATTGCTGGG-3′ and inserted as a *Sac*I-*Eco*RI fragment into pRS303-mKate. All plasmids were confirmed by sequence analysis.

Fluorescence microscopy and analysis

Cell imaging was performed at 25°C with a Zeiss Axio Imager M1 microscope (Carl Zeiss, Jena, Germany) with a mercury arc lamp and a 100×/1.30 numerical aperture oil immersion objective, and images were captured with an Orca-ER digital camera (Hamamatsu, Bridgewater, NJ) coupled to Openlab Software 5.0.1 (PerkinElmer-Cetus, Waltham, MA). A 475/40 excitation and 530/50 emission filter set was used for GFP and fluorescein isothiocyanate (FITC)–concanavalin A (Sigma-Aldrich, St. Louis, MO) images, and a 560/40 excitation and 630/75 emission filter set was used for RFP and rhodamine-phalloidin (Invitrogen, Carlsbad, CA) images.

For calcineurin localization studies, Cna1-3GFP was grown to mid log phase in synthetic complete dextrose (SCD), and hyperosmotic stress was initiated by adding NaCl, KCl, sorbitol, $CaCl_2$, or LiCl. Cells were concentrated by centrifugation and imaged. Cells were scored as having foci or bud neck/bud tip staining by eye, and >100 budded cells were counted at each time point; for statistical analysis, a one-phase decay was fitted to each time series with Prism (GraphPad, La Jolla, CA) and the two fits were compared with the extra sum-of-squares *F* test.

For the latrunculin A experiments, Cna1-3GFP cells were grown to mid log phase in SCD, synchronized with 15 μg/ml α-factor for 2 h, and then washed and released into SCD for 40 min. Latrunculin A (Sigma-Aldrich) stock solution was 20 mM in dimethyl sulfoxide (DMSO); cells were treated with 200 μM latrunculin A or 1% DMSO for 10 min, and then an equal volume of SCD with 2.5 M KCl and 200 μM latrunculin A or DMSO was added for an additional 10 min, at which point cells were imaged or fixed with 3.7% formaldehyde and stained with rhodamine–phalloidin (Invitrogen). Quantification of Cna1-3GFP from unfixed cells, $N > 100$, was conducted using ImageJ (National Institutes of Health, Bethesda MD): pixel intensity along a line parallel to the mother–bud axis and centered at the bud neck was averaged.

Actin polarization and GFP-2xPH(PLCδ) were measured in BY4741 and LSY312(InpΔΔΔ) cells. BY4741 cells were grown to mid log phase, and LSY312(InpΔΔΔ) were grown to saturation in selective media with 2% galactose and then washed and grown in 2% dextrose for at least 10 doublings. Cells were pretreated for between 30 min and 2 h with or without FK506, as indicated, and hyperosmotic stress was initiated by adding KCl to 1.25 M.

For actin polarization measurements, cells were fixed with 3.7% formaldehyde buffered with 100 mM KPi, pH 6.5, and stained with FITC-concanavalin A and rhodamine–phalloidin. Images were analyzed with CalMorph (http://scmd.gi.k.u-tokyo.ac.jp/datamine/calmorph/; Ohtani *et al.*, 2004), and actin polarity was calculated for small- and medium-budded cells as the ratio of actin brightness in the bud to actin brightness in the mother cell. Differences between distributions of actin polarity were evaluated for significance with the Kruskal–Wallis rank sum test for multiple comparisons using the MATLAB statistics tool pack (MathWorks, Natick, MA).

GFP-2xPH(PLCδ) invaginations (Figure 6) were measured with a custom membrane identification algorithm implemented in MATLAB; briefly, we used a Laplacian of Gaussian kernel to identify contours defining the inner and outer borders of the cell membrane and restricted the analysis to well-defined cells. Number of large invaginations was defined as the number of membrane regions identified that extended >10 pixels (~0.5 μm) from the outer edge of the cell. LSY312(InpΔΔΔ) cells with pRS426-Inp53, pRS316, pRS316-Inp53, and pRS316-Inp53^{ARAQAA} were treated with or without KCl for 10 min before imaging; >200 cells from each condition from three independent experiments were analyzed.

GFP-2xPH(PLCδ) enrichment/depletion (Figure 7) in wild-type (BY4741) cells, pretreated with FK506 or vehicle for 30 min with or without osmotic shock, was analyzed using a custom MATLAB script; we identified cell bodies and defined the outside five pixels as the membrane region; GFP enrichment relative to the adjacent cytoplasm was calculated in a sliding window along the membrane: a location on the membrane was scored as GFP enriched if the average fluorescence in the surrounding 10×5 pixel membrane region was >10% more than the average fluorescence in a similarly sized adjoining region of cytoplasm after image-wide background correction. Details and code are available on request. Statistical testing was with one-way analysis of variance (ANOVA) and Tukey's multiple comparison posttest (Prism), and >700 cells were analyzed from each condition from four independent experiments.

Analysis of correlation between Cna1-3GFP, Abp1-RFP, Inp53-3RFP, and Inp53^{ARAQAA}-3RFP was conducted as follows. Cell bodies were identified from fluorescence images by Otsu's threshold method. Pearson's *r* was determined for each GFP-RFP pair from all pixels in cell bodies. To calculate statistical significance, correlation scores from >10 images from at least two independent experiments were analyzed by one-way ANOVA with Tukey's posttest in Prism.

Mass spectrometry

Stable isotope labeling by amino acids in cell culture triple labeling was conducted following Gruhler and Kratchmarova (2008); cells were grown in minimal media supplemented with 30 mg/l in 1.3-l cultures. YEG1 was grown with Lys_0 (L-lysine), and YEG2 was grown with Lys_{+4} or Lys_{+8} (4,4,5,5-D4 L-lysine or U-13C6, U-15N2 L-lysine; Cambridge Isotope Laboratories, Andover MA). Cells were grown to OD of 0.8; 121 g of KCl was added to the Lys_8/YEG2 culture (1.25 M) for 10 min. Cells were washed, equalized by OD_{600}, and pooled, then resuspended in lysis buffer (100 mM

NaCl, 20 mM Tris, pH 7.6, 2 mM EDTA, 0.5% Triton, 1 mM dithiothreitol [DTT], and protease inhibitors [phenylmethylsulfonyl fluoride, aprotinin, leupeptin, pepstatin, benzamidine]), and droplets were frozen directly in liquid N_2. Frozen cell droplets were lysed with a Retsch MM301 Ball-Mill (5 ×2 min, 20 Hz, N2(l) cooled), and then extracts were clarified with 10,000, 50,000, and 100,000 × *g* spins. Cna2-S-TEV-ZZ and associated proteins were purified with immunoglobulin G (IgG)–Sepharose and eluted by TEV cleavage at 4°C (reaction buffer: 50 mM Tris, pH 8, 0.5 mM EDTA, 1 mM DTT, 50 U AcTEV [Invitrogen]; elution buffer: 250 mM NaCl, 20 mM Tris, pH 7.6, 2 mM EDTA, 0.5% Triton, 1 mM DTT). Eluted proteins were trichloroacetic acid (TCA) precipitated (15% TCA, –20°C overnight; washed three times with acetone), digested with LysC (50 mM ammonium bicarbonate, 10% acetonitrile, 20 ng/µl LysC, 37°C overnight; stop with 10% trifluoroacetic acid), and cleaned with a C18 StageTip as described (Rappsilber *et al.*, 2007; wash, 5% formic acid; elute, 50% acetonitrile, 5% formic acid). Samples were analyzed by liquid chromatography–tandem mass spectrometry (LTQ-Velos Orbitrap; Thermo Scientific, Waltham, MA). Peptides were identified with the SEQUEST algorithm (Yates *et al.*, 1995), against the yeast proteome concatenated with reversed decoy sequences and quantified with the VISTA algorithm (Bakalarski *et al.*, 2008).

Yeast protein purification and Western blotting

Copurification and Western blot studies with GST-tagged Inp53, Inp53^{ARAQAA}, and Inp53-SAC and IP5P and PRD domains were conducted in JRY11, BY4741, and Rvs167-GFP, Bsp1-GFP, Bzz1-GFP, and Sla1-GFP cells transformed with the appropriate plasmids. Cells were grown in synthetic complete (SC)–Ura 2% raffinose medium to mid log phase and treated with 1 µg/ml FK506 for 30 min where indicated and then induced with 2% galactose for 4 h. A 10-min hyperosmotic stress was induced by adding KCl to 1.25 M where indicated. Cells were harvested and washed in prechilled medium containing FK506 and 1.25 M KCl where appropriate and then pelleted and flash frozen in liquid N_2. Cells were resuspended in copurification buffer (150 mM NaCl, 20 mM Tris 7.6, 2 mM EDTA, 0.5% Triton X-100, 1 mM DTT, and protease inhibitors, with or without FK506 as appropriate) and were lysed with glass bead lysis, and extracts were clarified with 5000 and 20,000 × *g* spins; extracts were incubated with glutathione-Sepharose beads (GE Healthcare, Little Chalfont, United Kingdom) at 4°C for 2 h with end-over-end rotation and washed three times for 5 min in copurification buffer. Samples were boiled in 2× SDS loading buffer for 10 min at 95°C, resolved with SDS–PAGE using standard methods, and transferred to nitrocellulose membranes (Bio-Rad, Hercules, CA) for Western blotting. Membranes were blocked with SuperBlock (Thermo Scientific, Rockford, IL) and probed with rabbit polyclonal anti-GFP IgG fraction (Invitrogen), anti-S (a gift from Ron Kopito, Stanford University), anti-Chc1 (SKL-1, a gift from Greg Payne, University of California, Los Angeles), anti-Inp53 (a gift from John York, Vanderbilt Univeresity), anti-phosphoS/T/Y (Invitrogen, Beverly, MA), or mouse monoclonal anti-GST (Covance, Berkeley, CA) antibodies. Anti-rabbit or anti-mouse secondary antibodies conjugated to horseradish peroxidase (GE Healthcare) and SuperSignal West Dura Extended Duration Substrate (Thermo Scientific, Rockford, IL) or ECL Western Blotting Substrate (Pierce, Rockford, IL) were used to visualize proteins on Biomax XAR film (Eastman Kodak, Rochester, NY), except in Supplemental Figures S3 and S4, where anti-rabbit Alexa 780 and anti-mouse Alexa 680 secondary antibodies (Invitrogen) were visualized with an Odyssey scanner (LI-COR Biosciences, Lincoln, NE).

In vitro phosphatidylinositol phosphatase assays

For purification of Inp53 for in vitro assays, we transformed JRY11 with pEG6 (GST-Inp53wt) and grew cells to mid log phase in SC-Ura 2% raffinose medium and treated with or without 1 µg/ml FK506 for 30 min and then induced with 2% galactose for 4 h. A 10-min hyperosmotic stress was induced by adding KCl to 1.25 M. A 500-ml amount of cells was harvested and washed in prechilled medium containing FK506 and 1.25 M KCl where appropriate, then resuspended in lysis buffer (150 mM NaCl, 20 mM Tris, pH 7.6, 2 mM EDTA, 1 mM DTT, 5 mM Na pyrophosphate, protease inhibitors). To preserve SAC domain activity (with or without FK506), no detergent was used and droplets were frozen directly in liquid N_2. Frozen cell droplets were lysed with a Retsch MM301 Ball-Mill (5 ×2 min, 20 Hz, N2(l) cooled), and then extracts were clarified at 5000 and 20,000 × *g*. GST-Inp53 was purified with glutathione-Sepharose beads (GE Healthcare) for 2 h at 4°C with end-over-end rotation and washed three times for 5 min, then eluted with 150 mM NaCl, 50 mM Tris, pH 7.6, 40 mM glutathione, and 1 mM DTT and dialyzed with 50 mM Tris, pH 7.6, 1 mM DTT, and frozen with 15% glycerol at –80°C. Proteins were analyzed by SDS–PAGE and Coomassie stained to assess purity or transferred to polyvinylidene fluoride membrane and Western blotted with mouse monoclonal anti-GST primary (Covance, Emeryville, CA) and anti-mouse Alexa 680 secondary antibodies (Invitrogen); immunoblots were observed with an Odyssey scanner, and relative protein amounts were calculated from serial dilutions using ImageJ (unpublished data). Equal amounts of each enzyme were used (approximately 10 nM) for each reaction. Phosphatidylinositol phosphatase activity was assayed in 50 mM 4-(2-hydroxyethyl)-1-piperazineethanesulfonic acid, pH 7.4, 50 mM KCl, 3 mM ethylene glycol tetraacetic acid, and 2 mM $MgCl_2$, with 0–250 µM di-C8-phoshatidylinositol(4,5)bis-phosphate (Echelon Biosciences, Salt Lake City UT); phosphate release was measured with Biomol Green (Enzo Life Sciences, Farmingdale, NY); rates were calculated from at least four linear time points and fitted with an allosteric-sigmoidal model and tested for significance with an extra sum-of-squares *F* test ($p < 0.13$, one curve adequately explained all data).

ACKNOWLEDGMENTS

We thank John York, Maria Molina, and Ron Kopito for reagents. We thank the members of the Cyert lab for helpful discussion. This work was supported by National Institutes of Health Grants GM-48728 (M.S.C., A.R.G.) and T32-GM007276 (E.L.G.), by a Tom and Susan Ford Stanford Graduate Fellowship (E.L.G.), and by the Stanford School of Medicine Jill and John Freidenrich Translational Medicine Fund (J.E.E.).

REFERENCES

Aghamohammadzadeh S, Ayscough KR (2009). Differential requirements for actin during yeast and mammalian endocytosis. Nat Cell Biol 11, 1039–1042.

Aguilar PS, Frohlich F, Rehman M, Shales M, Ulitsky I, Olivera-Couto A, Braberg H, Shamir R, Walter P, Mann M, *et al.* (2010). A plasma-membrane E-MAP reveals links of the eisosome with sphingolipid metabolism and endosomal trafficking. Nat Struct Mol Biol 17, 901–908.

Alvaro CG, O'Donnell AF, Prosser DC, Augustine AA, Goldman A, Brodsky JL, Cyert MS, Wendland B, Thorner J (2014). Specific alpha-arrestins negatively regulate Saccharomyces cerevisiae pheromone response by down-modulating the G-protein coupled receptor Ste2. Mol Cell Biol 34, 2660–2681.

Ausubel FM, Brent R, Kingston RE, Moore DE, Smith SA, Struhl K, eds. (1991). Current Protocols in Molecular Biology, New York: John Wiley & Sons.

Bakalarski CE, Elias JE, Villen J, Haas W, Gerber SA, Everley PA, Gygi SP (2008). The impact of peptide abundance and dynamic range on

stable-isotope-based quantitative proteomic analyses. J Proteome Res 7, 4756–4765.
Balguerie A, Bagnat M, Bonneu M, Aigle M, Breton AM (2002). Rvs161p and sphingolipids are required for actin repolarization following salt stress. Eukaryot Cell 1, 1021–1031.
Bauer F, Urdaci M, Aigle M, Crouzet M (1993). Alteration of a yeast SH3 protein leads to conditional viability with defects in cytoskeletal and budding patterns. Mol Cell Biol 13, 5070–5084.
Bi E, Park HO (2012). Cell polarization and cytokinesis in budding yeast. Genetics 191, 347–387.
Bonangelino CJ, Nau JJ, Duex JE, Brinkman M, Wurmser AE, Gary JD, Emr SD, Weisman LS (2002). Osmotic stress-induced increase of phosphatidylinositol 3,5-bisphosphate requires Vac14p, an activator of the lipid kinase Fab1p. J Cell Biol 156, 1015–1028.
Bultynck G, Heath VL, Majeed AP, Galan JM, Haguenauer-Tsapis R, Cyert MS (2006). Slm1 and slm2 are novel substrates of the calcineurin phosphatase required for heat stress-induced endocytosis of the yeast uracil permease. Mol Cell Biol 26, 4729–4745.
Chowdhury S, Smith KW, Gustin MC (1992). Osmotic stress and the yeast cytoskeleton: phenotype-specific suppression of an actin mutation. J Cell Biol 118, 561–571.
Clayton EL, Anggono V, Smillie KJ, Chau N, Robinson PJ, Cousin MA (2009). The phospho-dependent dynamin-syndapin interaction triggers activity-dependent bulk endocytosis of synaptic vesicles. J Neurosci 29, 7706–7717.
Clayton EL, Cousin MA (2009). The molecular physiology of activity-dependent bulk endocytosis of synaptic vesicles. J Neurochem 111, 901–914.
Cousin MA (2009). Activity-dependent bulk synaptic vesicle endocytosis—a fast, high capacity membrane retrieval mechanism. Mol Neurobiol 39, 185–189.
Cyert MS, Kunisawa R, Kaim D, Thorner J (1991). Yeast has homologs (CNA1 and CNA2 gene products) of mammalian calcineurin, a calmodulin-regulated phosphoprotein phosphatase. Proc Natl Acad Sci USA 88, 7376–7380.
Cyert MS, Philpott CC (2013). Regulation of cation balance in Saccharomyces cerevisiae. Genetics 193, 677–713.
Daboussi L, Costaguta G, Payne GS (2012). Phosphoinositide-mediated clathrin adaptor progression at the trans-Golgi network. Nat Cell Biol 14, 239–248.
Denis V, Cyert MS (2002). Internal Ca(2+) release in yeast is triggered by hypertonic shock and mediated by a TRP channel homologue. J Cell Biol 156, 29–34.
Di Pietro SM, Cascio D, Feliciano D, Bowie JU, Payne GS (2010). Regulation of clathrin adaptor function in endocytosis: novel role for the SAM domain. EMBO J 29, 1033–1044.
Dudley AM, Janse DM, Tanay A, Shamir R, Church GM (2005). A global view of pleiotropy and phenotypically derived gene function in yeast. Mol Syst Biol 1, 2005.0001.
Dupont S, Beney L, Ritt J-F, Lherminier J, Gervais P (2010). Lateral reorganization of plasma membrane is involved in the yeast resistance to severe dehydration. Biochim Biophys Acta 1798, 975–985.
Evans GJ, Cousin MA (2007). Activity-dependent control of slow synaptic vesicle endocytosis by cyclin-dependent kinase 5. J Neurosci 27, 401–411.
Feliciano D, Di Pietro SM (2012). SLAC, a complex between Sla1 and Las17, regulates actin polymerization during clathrin-mediated endocytosis. Mol Biol Cell 23, 4256–4272.
Goldman AR, Roy J, Bodenmiller B, Wanka S, Landry CR, Aebersold R, Cyert MS (2014). The calcineurin signaling network evolves via conserved kinase-phosphatase modules that transcend substrate identity. Mol Cell 55, 422–435.
Grigoriu S, Bond R, Cossio P, Chen JA, Ly N, Hummer G, Page R, Cyert MS, Peti W (2013). The molecular mechanism of substrate engagement and immunosuppressant inhibition of calcineurin. PLoS Biol 11, e1001492.
Gruhler S, Kratchmarova I (2008). Stable isotope labeling by amino acids in cell culture (SILAC). Methods Mol Biol 424, 101–111.
Guo S, Stolz LE, Lemrow SM, York JD (1999). SAC1-like domains of yeast SAC1, INP52, and INP53 and of human synaptojanin encode polyphosphoinositide phosphatases. J Biol Chem 274, 12990–12995.
Ha SA, Bunch JT, Hama H, DeWald DB, Nothwehr SF (2001). A novel mechanism for localizing membrane proteins to yeast trans-Golgi network requires function of synaptojanin-like protein. Mol Biol Cell 12, 3175–3190.
Ha SA, Torabinejad J, DeWald DB, Wenk MR, Lucast L, De Camilli P, Newitt RA, Aebersold R, Nothwehr SF (2003). The synaptojanin-like protein Inp53/Sjl3 functions with clathrin in a yeast TGN-to-endosome pathway distinct from the GGA protein-dependent pathway. Mol Biol Cell 14, 1319–1333.
Johnson ME, Hummer G (2013). Interface-resolved network of protein-protein interactions. PLoS Comput Biol 9, e1003065.
Juvvadi PR, Fortwendel JR, Rogg LE, Burns KA, Randell SH, Steinbach WJ (2011). Localization and activity of the calcineurin catalytic and regulatory subunit complex at the septum is essential for hyphal elongation and proper septation in Aspergillus fumigatus. Mol Microbiol 82, 1235–1259.
Kaksonen M, Toret CP, Drubin DG (2005). A modular design for the clathrin- and actin-mediated endocytosis machinery. Cell 123, 305–320.
Kishimoto T, Sun Y, Buser C, Liu J, Michelot A, Drubin DG (2011). PNAS Plus: determinants of endocytic membrane geometry, stability, and scission. Proc Natl Acad Sci USA 108, E979–E988.
Kittelmann M, Liewald JF, Hegermann J, Schultheis C, Brauner M, Steuer Costa W, Wabnig S, Eimer S, Gottschalk A (2013). In vivo synaptic recovery following optogenetic hyperstimulation. Proc Natl Acad Sci USA 110, E3007–E3016.
Kopecka M, Svoboda A, Brichta J (1973). Effect of "osmotic stabilizers" and glycerol on yeast cell envelopes. Z Allg Mikrobiol 13, 481–487.
Kozubowski L, Aboobakar EF, Cardenas ME, Heitman J (2011). Calcineurin colocalizes with P-bodies and stress granules during thermal stress in Cryptococcus neoformans. Eukaryot Cell 10, 1396–1402.
Lee J, Reiter W, Dohnal I, Gregori C, Beese-Sims S, Kuchler K, Ammerer G, Levin DE (2013). MAPK Hog1 closes the S. cerevisiae glycerol channel Fps1 by phosphorylating and displacing its positive regulators. Genes Dev 27, 2590–2601.
Levin DE (2011). Regulation of cell wall biogenesis in Saccharomyces cerevisiae: the cell wall integrity signaling pathway. Genetics 189, 1145–1175.
Liu J, Sun Y, Drubin DG, Oster GF (2009). The mechanochemistry of endocytosis. PLoS Biol 7, e1000204.
Loewith R, Hall MN (2011). Target of rapamycin (TOR) in nutrient signaling and growth control. Genetics 189, 1177–1201.
Mahadev RK, Di Pietro SM, Olson JM, Piao HL, Payne GS, Overduin M (2007). Structure of Sla1p homology domain 1 and interaction with the NPFxD endocytic internalization motif. EMBO J 26, 1963–1971.
Manford A, Xia T, Saxena AK, Stefan C, Hu F, Emr SD, Mao Y (2010). Crystal structure of the yeast Sac1: implications for its phosphoinositide phosphatase function. EMBO J 29, 1489–1498.
Mani M, Lee SY, Lucast L, Cremona O, Di Paolo G, De Camilli P, Ryan TA (2007). The dual phosphatase activity of synaptojanin1 is required for both efficient synaptic vesicle endocytosis and reavailability at nerve terminals. Neuron 56, 1004–1018.
Mendoza I, Rubio F, Rodriguez-Navarro A, Pardo JM (1994). The protein phosphatase calcineurin is essential for NaCl tolerance of Saccharomyces cerevisiae. J Biol Chem 269, 8792–8796.
Meunier FA, Wenzel EM, Morton A, Ebert K, Welzel O, Kornhuber J, Cousin MA, Groemer TW (2012). Key physiological parameters dictate triggering of activity-dependent bulk endocytosis in hippocampal synapses. PLoS One 7, e38188.
Miermont A, Waharte F, Hu S, McClean MN, Bottani S, Léon S, Hersen P (2013). Severe osmotic compression triggers a slowdown of intracellular signaling, which can be explained by molecular crowding. Proc Natl Acad Sci USA 110, 5725–5730.
Morris GJ, Winters L, Coulson GE, Clarke KJ (1986). Effect of osmotic stress on the ultrastructure and viability of the yeast Saccharomyces cerevisiae. J Gen Microbiol 132, 2023–2034.
Mulholland J, Preuss D, Moon A, Wong A, Drubin D, Botstein D (1994). Ultrastructure of the yeast actin cytoskeleton and its association with the plasma membrane. J Cell Biol 125, 381–391.
Nanduri J, Tartakoff AM (2001a). The arrest of secretion response in yeast: signaling from the secretory path to the nucleus via Wsc proteins and Pkc1p. Mol Cell 8, 281–289.
Nanduri J, Tartakoff AM (2001b). Perturbation of the nucleus: a novel Hog1p-independent, Pkc1p-dependent consequence of hypertonic shock in yeast. Mol Biol Cell 12, 1835–1841.
O'Donnell AF, Huang L, Thorner J, Cyert MS (2013). A calcineurin-dependent switch controls the trafficking function of alpha-arrestin Aly1/Art6. J Biol Chem 288, 24063–24080.
Ohtani M, Saka A, Sano F, Ohya Y, Morishita S (2004). Development of image processing program for yeast cell morphology. J Bioinform Comput Biol 1, 695–709.
Oliveria SF, Dell'Acqua ML, Sather WA (2007). AKAP79/150 anchoring of calcineurin controls neuronal L-type Ca2+ channel activity and nuclear signaling. Neuron 55, 261–275.

Ooms LM, McColl BK, Wiradjaja F, Wijayaratnam AP, Gleeson P, Gething MJ, Sambrook J, Mitchell CA (2000). The yeast inositol polyphosphate 5-phosphatases inp52p and inp53p translocate to actin patches following hyperosmotic stress: mechanism for regulating phosphatidylinositol 4,5-bisphosphate at plasma membrane invaginations. Mol Cell Biol 20, 9376–9390.
Palmer RE, Sullivan DS, Huffaker T, Koshland D (1992). Role of astral microtubules and actin in spindle orientation and migration in the budding yeast, Saccharomyces cerevisiae. J Cell Biol 119, 583–593.
Piao HL, Machado IM, Payne GS (2007). NPFXD-mediated endocytosis is required for polarity and function of a yeast cell wall stress sensor. Mol Biol Cell 18, 57–65.
Pruyne D, Gao L, Bi E, Bretscher A (2004). Stable and dynamic axes of polarity use distinct formin isoforms in budding yeast. Mol Biol Cell 15, 4971–4989.
Rappsilber J, Mann M, Ishihama Y (2007). Protocol for micro-purification, enrichment, pre-fractionation and storage of peptides for proteomics using StageTips. Nat Protoc 2, 1896–1906.
Roy J, Cyert MS (2009). Cracking the phosphatase code: docking interactions determine substrate specificity. Sci Signal 2, re9.
Roy J, Cyert MS (2013). Calcineurin. In: Encyclopedia of Metalloproteins, ed. RH Kretsinger, VN Uversky, and EA Permyakov, New York: Springer, 392–402.
Roy J, Li H, Hogan PG, Cyert MS (2007). A conserved docking site modulates substrate affinity for calcineurin, signaling output, and in vivo function. Mol Cell 25, 889–901.
Saheki Y, De Camilli P (2012). Synaptic vesicle endocytosis. Cold Spring Harbor Perspect Biol 4, a005645.
Saito H, Posas F (2012). Response to hyperosmotic stress. Genetics 192, 289–318.
Schaber J, Adrover MA, Eriksson E, Pelet S, Petelenz-Kurdziel E, Klein D, Posas F, Goksor M, Peter M, Hohmann S, Klipp E (2010). Biophysical properties of Saccharomyces cerevisiae and their relationship with HOG pathway activation. Eur Biophys J 39, 1547–1556.
Shcherbo D, Merzlyak EM, Chepurnykh TV, Fradkov AF, Ermakova GV, Solovieva EA, Lukyanov KA, Bogdanova EA, Zaraisky AG, Lukyanov S, Chudakov DM (2007). Bright far-red fluorescent protein for whole-body imaging. Nat Methods 4, 741–746.
Sherman F (1991). Getting started with yeast. Methods Enzymol 194, 3–21.
Shupliakov O, Low P, Grabs D, Gad H, Chen H, David C, Takei K, De Camilli P, Brodin L (1997). Synaptic vesicle endocytosis impaired by disruption of dynamin-SH3 domain interactions. Science 276, 259–263.
Singer-Kruger B, Nemoto Y, Daniell L, Ferro-Novick S, De Camilli P (1998). Synaptojanin family members are implicated in endocytic membrane traffic in yeast. J Cell Sci 111, 3347–3356.
Slaninova I, Sestak S, Svoboda A, Farkas V (2000). Cell wall and cytoskeleton reorganization as the response to hyperosmotic shock in Saccharomyces cerevisiae. Arch Microbiol 173, 245–252.
Smaczynska-de RII, Allwood EG, Aghamohammadzadeh S, Hettema EH, Goldberg MW, Ayscough KR (2010). A role for the dynamin-like protein Vps1 during endocytosis in yeast. J Cell Sci 123, 3496–3506.
Smaczynska-de RII, Allwood EG, Mishra R, Booth WI, Aghamohammadzadeh S, Goldberg MW, Ayscough KR (2012). Yeast dynamin Vps1 and amphiphysin Rvs167 function together during endocytosis. Traffic 13, 317–328.
Soulard A, Lechler T, Spiridonov V, Shevchenko A, Li R, Winsor B (2002). Saccharomyces cerevisiae Bzz1p is implicated with type I myosins in actin patch polarization and is able to recruit actin-polymerizing machinery in vitro. Mol Cell Biol 22, 7889–7906.
Srinivasan S, Seaman M, Nemoto Y, Daniell L, Suchy SF, Emr S, De Camilli P, Nussbaum R (1997). Disruption of three phosphatidylinositol-polyphosphate 5-phosphatase genes from Saccharomyces cerevisiae results in pleiotropic abnormalities of vacuole morphology, cell shape, and osmohomeostasis. Eur J Cell Biol 74, 350–360.
Stathopoulos AM, Cyert MS (1997). Calcineurin acts through the CRZ1/TCN1-encoded transcription factor to regulate gene expression in yeast. Genes Dev 11, 3432–3444.
Stathopoulos-Gerontides A, Guo JJ, Cyert MS (1999). Yeast calcineurin regulates nuclear localization of the Crz1p transcription factor through dephosphorylation. Genes Dev 13, 798–803.
Stefan CJ, Audhya A, Emr SD (2002). The yeast synaptojanin-like proteins control the cellular distribution of phosphatidylinositol (4,5)-bisphosphate. Mol Biol Cell 13, 542–557.
Stefan CJ, Padilla SM, Audhya A, Emr SD (2005). The phosphoinositide phosphatase Sjl2 Is recruited to cortical actin patches in the control of vesicle formation and fission during endocytosis. Mol Cell Biol 25, 2910–2923.
Stolz LE, Huynh CV, Thorner J, York JD (1998). Identification and characterization of an essential family of inositol polyphosphate 5-phosphatases (INP51, INP52 and INP53 gene products) in the yeast Saccharomyces cerevisiae. Genetics 148, 1715–1729.
Sun Y, Carroll S, Kaksonen M, Toshima JY, Drubin DG (2007). PtdIns(4,5)P2 turnover is required for multiple stages during clathrin- and actin-dependent endocytic internalization. J Cell Biol 177, 355–367.
Sun Y, Martin AC, Drubin DG (2006). Endocytic internalization in budding yeast requires coordinated actin nucleation and myosin motor activity. Dev Cell 11, 33–46.
Taylor MJ, Perrais D, Merrifield CJ (2011). A high precision survey of the molecular dynamics of mammalian clathrin-mediated endocytosis. PLoS Biol 9, e1000604.
Tonikian R, Xin X, Toret CP, Gfeller D, Landgraf C, Panni S, Paoluzi S, Castagnoli L, Currell B, Seshagiri S, *et al.* (2009). Bayesian modeling of the yeast SH3 domain interactome predicts spatiotemporal dynamics of endocytosis proteins. PLoS Biol 7, e1000218.
Utsugi T, Minemura M, Hirata A, Abe M, Watanabe D, Ohya Y (2002). Movement of yeast 1,3-beta-glucan synthase is essential for uniform cell wall synthesis. Genes Cells 7, 1–9.
Wapinski I, Pfeffer A, Friedman N, Regev A (2007). Natural history and evolutionary principles of gene duplication in fungi. Nature 449, 54–61.
Weinberg J, Drubin DG (2012). Clathrin-mediated endocytosis in budding yeast. Trends Cell Biol 22, 1–13.
Wicky S, Frischmuth S, Singer-Krüger B (2003). Bsp1p/Ypr171p is an adapter that directly links some synaptojanin family members to the cortical actin cytoskeleton in yeast. FEBS Lett 537, 35–41.
Winther AM, Jiao W, Vorontsova O, Rees KA, Koh TW, Sopova E, Schulze KL, Bellen HJ, Shupliakov O (2013). The dynamin-binding domains of Dap160/intersectin affect bulk membrane retrieval in synapses. J Cell Sci 126, 1021–1031.
Xin X, Gfeller D, Cheng J, Tonikian R, Sun L, Guo A, Lopez L, Pavlenco A, Akintobi A, Zhang Y, *et al.* (2013). SH3 interactome conserves general function over specific form. Mol Syst Biol 9, 652.
Yates JR 3rd, Eng JK, McCormack AL, Schieltz D (1995). Method to correlate tandem mass spectra of modified peptides to amino acid sequences in the protein database. Anal Chem 67, 1426–1436.
Yoshikawa K, Tanaka T, Furusawa C, Nagahisa K, Hirasawa T, Shimizu H (2009). Comprehensive phenotypic analysis for identification of genes affecting growth under ethanol stress in Saccharomyces cerevisiae. FEMS Yeast Res 9, 32–44.
Yuzyuk T (2002). The MEK kinase Ssk2p promotes actin cytoskeleton recovery after osmotic stress. Mol Biol Cell 13, 2869–2880.
Yuzyuk T (2003). Actin recovery and bud emergence in osmotically stressed cells requires the conserved actin interacting mitogen-activated protein kinase kinase kinase Ssk2p/MTK1 and the scaffold protein Spa2p. Mol Biol Cell 14, 3013–3026.